LEVEL II

12
B.S.

ENERGY LABORATORY
AND
CERAMICS PROCESSING
RESEARCH LABORATORY

MASSACHUSETTS INSTITUTE
OF TECHNOLOGY

SINTERABLE POWDERS FROM LASER DRIVEN REACTIONS

BY

John S. Haggerty
W. Roger Cannon

October 1978

Energy Laboratory Report
MIT-EL-78-037

BUILDING NO. 12
MASSACHUSETTS INSTITUTE OF TECHNOLOGY
CAMBRIDGE, MASSACHUSETTS 02139

(6) SINTERABLE POWDERS FROM LASER DRIVEN REACTIONS.

(10) John S. Haggerty
[redacted]

W. Roger Cannon
Dept. of Materials Science and Engineering

Massachusetts Institute of Technology
Cambridge, Massachusetts 02139

(11) Oct[redacted]78 (12) 82 p.

(14) MIT-EL-78-037

Prepared for:

The U. S. Department of Defense

ARPA order No: 3449
Program Code No.: NR039-153
(15) Contract No.: N00014-77-C-0581, ARPA Order-3449
Contract Date: 1 July 1977
Contract Expiration Date: 30 June 1979
Contract Amount: $256,580.00
(9) Status Report Period: 1 July [redacted]77-30 Jun[redacted]978

The views and conclusions contained in this document are those of the authors and should not be interpreted as necessarily representing the official policies, either expressed of implied of the Defense Advanced Research Projects Agency or the U. S. Government.

TABLE OF CONTENTS

LIST OF FIGURES

LIST OF TABLES

Abstract

Novel methods for producing ideal powders for fabricating Si_3N_4 ceramic parts have been investigated. The characteristics sought were principally uniformly small diameter, equiaxed, high purity particles which are free of agglomerates. Two laser processes were studied.

In the first, a CO_2 laser source was used to heat the reactant gases by coupling directly to them. Silicon (Si) and Si_3N_4 powders have been synthesized directly from SiH_4 and NH_3/SiH_4 mixtures respectively. The spatially well-defined reaction zone and the combination of the rapid heating rates with the short times at reaction temperatures yielded very uniform and small diameter particles. Si_3N_4 powders were produced with particle diameters entirely within the range of 100-200 Å. The particles are equiaxed and nearly spherical. The Si powders had the same general characteristics, but exhibited a slightly larger range of diameters.

An analytical model gives an approximate description of the process. The reaction proceeds as a thermal reaction at thresholds which agree with measured optical absorptivities. The absorptivities are high, which will permit good efficiencies to be achieved. We were not successful in inducing a multiphoton, unimolecular reaction.

The second process uses selective heating to reduce the size of oversized particles or agglomerates as well as modifying the shape of high aspect ratio particles. This process is based on the decreasing absorption efficiency of a particle to light when its diameter is less than the wavelength of the incident light. Light induced comminution was demonstrated.

The power required for comminution is higher than was originally anticipated, but it agrees with present analytical models. While the process was domonstrated with a 150 watt CO_2 laser, this power limitation precluded an orderly investigation of process variables. It appears that 750-1500 watts are required to operate continuously. These and higher power CO_2 lasers are commercially available.

We have successfully demonstrated both processes for producing superior Si and Si_3N_4 powders. The results of the direct synthesis approach are viewed as extremely important. Their uniform, small particle sizes make them unique with respect to all other powders. While demonstrated with Si and Si_3N_4 powders, the process appears applicable to other materials. More work is required to determine the ultimate significance of the laser commintion process. It appears that the process will work as anticipated and will induce the desired size and shape changes. It is apparent that it will be an energy intensive process.

Forward

This research program has involved several groups within M.I.T., which represent different technical disciplines. The principal investigators, Drs. J. S. Haggerty and W. R. Cannon, are materials scientists associated with both the Energy Laboratory and The Department of Materials Science and Engineering. Dr. S. Danforth, who has worked on all aspects of this program is associated with the Department of Materials Science and Engineering. Professor C. F. Dewey and Mr. J. H. Flint, who conducted the absorptivity and threshold experiments, are members of the Mechanical Engineering Department staff. Mr. C. Reiser, who investigated the feasibility of inducing unimolecular reactions, is a Research Assistant in the Chemistry Department. The novelty of these processes for using lasers to produce ideal powders has intrinsically required an interdisciplinary approach.

I. Introduction

It was well established by Coble[1] twenty years ago that ceramic materials could be densified by diffusional sintering processes to theoretical density provided important criteria were satisfied. The paradigms for this process have been established for oxides, but are less well defined and are even further from demonstration for the covalent materials such as silicon carbide and silicon nitride. Since the latter are being considered for high temperature structural applications, the requirements of theoretical density, uniform grain size, and elimination of flaws are fundamental to their eventual incorporation in power machinery. Without enumerating all of the justifications, an ideal sinterable powder (Si_3N_4) can be defined as one having the following characteristics: (1) fine grain size, less than 0.5 microns; (2) non-agglomerated particles, i.e., individual crystallites; (3) a narrow distribution in the sizes of the particles; (4) the morphology equiaxed, tending towards spherical; (5) phase purity, i.e., no mix of alpha and beta crystal structures; (6) compositional purity (less than 0.1%, except oxygen less than 2%). It is presumed that a powder with these ideal characteristics can be sintered to theoretical density without pressure or additives, and that the grain morphology could be controlled to give useful high temperature properties. If not, it will serve as an ideal research vehicle to learn how to achieve the desired sintering characteristics. Although there have been significant improvements in the characteristics of fine silicon nitride and silicon carbide powders in recent years, they still have many deficiencies. In this program, laser heat sources have been studied as means for synthesizing and modifying Si_3N_4 powders.

Most of the Si_3N_4 process techniques involve DC arcs, conventional vapor phase reactions in heated tube furnaces or nitriding or carbiding of silicon metal. The nitriding of silicon metal typically leaves a silicon core within the silicon nitride particle. Furthermore, because the process is done in the solid state, grinding and separating of particles is necessary, but this does not result in narrow size distribution, non-agglomerated, phase pure powders. The vapor phase method (the furnace heated vapor and the arc plasma techniques) yield a finer and more uniform powder than the nitriding of solid silicon; but from the point of view of studying the ultimate properties of materials formed from ideal powders, these techniques have less than ideal thermal profiles and reaction zones which allow for a distribution in nucleation and growth times and the

formation of agglomerates. Despite these specific process deficiencies, direct synthesis of powders from dilute gas phase reactants is the most promising route for producing ideal powders.

Laser driven gas phase reactions were proposed because of the advantages that this processing technique offers. It is a clean process which permits cold, non-reactive chamber walls. The reaction volume is very well-defined and consists only of that volume traversed by reaction gases and particles, i.e., the laser beam area. The ability to maintain steep temperature gradients in the effective thermal environment, and thus a well-defined reaction zone, should allow precise control of the nucleation rate, the growth rate and exposure times, permitting the nucleation and growth of very fine particles. The available power with a CO_2 laser, the stability of the delivered power, its cost, reliability and efficiency, allow for this to be a viable process which will yield improvements in fabrication of powders for these high performance materials. The use of this technique as an experimental tool has tremendous potential, and its eventual use as a production tool should also be considered.

Three specific laser means for synthesizing and modifying powders were proposed. The first technique involves the absorption of laser radiation by gas phase molecules and their subsequent reaction to form particles. The process is a homogeneous gas phase reaction. The advantages as mentioned above are a clean system, cold walls, and a controlled hot zone. The second primary technique is pyrolysis of a silicon reactant to form composite particles of silicon on silicon nitride. In this case, a silicon nitride particle would be heated, and provide a heterogeneous surface for a film of silicon deposition. The subsequent nitriding during reaction sintering would go to completion because the core would be silicon nitride. The third area involves comminution of particles and relates to both of the above primary research areas. The fundamental principle is that 10.6 μm wavelength CO_2 laser radiation couples with particles with diameters which are a micron or larger, but not with much smaller particles. In this way, vaporization of agglomerates or large particles causes the refinement in the particle size and size distribution. This also tends towards more equiaxed particles, as well as non-agglomerated ones. The first and third approaches have been studied during this first year report period.

II. Powder Synthesis from Gas Phase Reactants

A. Introduction

The overall objective of this portion of the program is to develop controllable processes for forming Si and Si_3N_4 powders directly from gas phase reactants using a laser as the source of energy. Experiments have been carried out both to develop empirical observations which describe the effect of process variables on the characteristics of resulting powders as well as providing missing property data. Models have been developed which provide an analytical description of the process.

The synthesis of Si and Si_3N_4 directly from gas phase reactants have been studied for a wide range of applications, from the very slow, carefully controlled conditions required for heteroepitaxial growth of thin film single crystals, to the severe and uncontrolled conditions experienced in various plasma techniques for forming powders. Most of the reported work with synthesis of Si_3N_4 powders has used high temperature tube furnaces[2,3] and plasmas,[4,5] with relatively little interest in Si powders.

This prior work with these materials provides a basis for understanding the thermodynamics and, to a lesser extent, the kinetics of the nucleation and growth processes involved in the synthesis of these powders. The extremely large heating rates and the different mechanisms of directly coupling to the gas phase reactants may reveal different rate controlling steps and reaction sequences with laser heating than has been observed with other heating techniques. Despite these differences, the prior work does provide important insights into this complex process.

One of the most complete studies of Si_3N_4 powder synthesis from gas phase reactants was reported by Prochazka and Greskovich.[2,6] They produced fine, spherical, reasonably stoichiometric silicon nitride powders from NH_3/SiH_4 mixtures in a high temperature pass-through furnace. These amorphous powders exhibited specific surface areas in the range of 4 to 80 m^2/g. The principal deficiency of this specific process is the wide range of particle sizes which were produced. Under typical conditions, particle diameters ranged from 300 to 2000 Å.

The laser heat source exhibits several interesting characteristics which have many advantages relative to other heat sources which have been investigated.

As noted previously, the power intensity and exposure time can be unusually well controlled, giving a precisely controlled time-temperature history. The large heating rates and short exposure times produce smaller particle sizes than are achieved by other processes. The absence of contaminants is another important feature. Unique reaction sequences may also result from preferentially coupling to one of the reactants. In the extreme, a multiphoton, unimolecular reaction might be induced which is only feasible with a laser heat source. Therefore, the laser energy source appeared important because it had a high probability of producing extremely small, uniform diameter particles which in their own right are unique. Additionally, the unique chemistry which is possible with the laser energy source offers the opportunity of achieving other important characteristics.

A CO_2 laser was selected for the initial investigation of synthesizing ceramic powders from gas phase reactants. These commercially available lasers emit high powers in pulsed and cw modes. These are important features for all aspects of process development ranging from research to the ultimate production of commercial quantities of powder. They can also be tuned to emit on many lines with wavelengths ranging from approximately 9.1 to 11.0 μm. Many of the candidate reactants have strong absorption bands in this wavelength range.

Silane (SiH_4) and ammonia (NH_3) were selected as reactants for the synthesis of Si and Si_3N_4 powders. This selection was based on prior successful experience with synthesizing silicon nitride using other energy sources to drive the chemical reactions. Overall these reactions proceed as

$$SiH_4 \rightarrow Si + 2H_2$$

and

$$3SiH_4 + 4NH_3 \rightarrow Si_3N_4 + 12H_2$$

Chlorine containing silicon sources, e.g., $SiCl_4$ and SiH_2Cl_2, etc., have also been used successfully, but their use in this program was deferred primarily because Morgan[7] reported that the sintering characteristics of Si_3N_4 powders were inhibited by retained chlorine. Also, spectrographic data indicated that both of the selected gases exhibited vibrational absorption bands very close to 10.6 μm, the approximate wavelength of the highest gain emissions (P(18) and P(20) lines) from the CO_2 laser.

The CO_2 laser emissions and the reported absorption peaks for SiH_4 and NH_3 are summarized in Fig. 1. Despite the profusion of absorption peaks which are extremely close to the emitted lines, this data cannot be used to estimate absorptivities. Unless the emission and absorption lines lie within a few doppler widths of one another (1 doppler width $\simeq 2\text{-}4 \times 10^{-5}$ μm), there will be virtually no coupling at low pressures. The resolution with which the absorption spectra were determined does not permit the location of the peaks to be stated with this precision. At higher temperatures and pressures, the actual peak widths are determined by subtle thermal and pressure broadening effects. The spectra appearing in the literature were not measured with sufficient precision to allow us to calculate absorptivities. Therefore, the actual absorptivities must be measured with laser sources and with gas conditions which are very close to those of interest for the reaction. No data of this type existed for SiH_4 and only one measurement was located for ammonia. For very dilute ammonia in one atmosphere of air, the absorptivities[10] were 0.14 and 0.12 $cm^{-1}atm^{-1}$ for the P(18) and P(20) emissions respectively. Absorptivity measurements were an essential part of the experimental program because their values are needed for modeling.

Two limiting types of laser induced dissociations of gases may be distinguished on the basis of the time scale in which the reaction occurs - a conventional thermal reaction and a unimolecular reaction. Thermal reactions are characterized by a normal thermal distribution of energies in vibrational, translational and rotational modes for all molecules. A unimolecular reaction is one in which a single molecule dissociates without interaction with other molecules. In a multiphoton unimolecular reaction, molecules absorb several laser photons as vibrational energy and dissociate before colliding with enough other molecules to develop a normal thermal distribution of translational, vibrational and rotational energies. Under these conditions, reactions are possible which would not be possible under thermal conditions alone. Between these two limiting cases, preferential coupling to one reactant combined with the usually large heating rates and short times may cause atypical reaction paths. The laser may interact selectively with a single, highly absorbing gas species in a mixture of gases if the other species are not highly absorbing, for instance silane in a silane-ammonia mixture. If enough energy can be absorbed by the silane molecule to dissociate before colliding with other molecules, a multiphoton, unimolecular reaction can

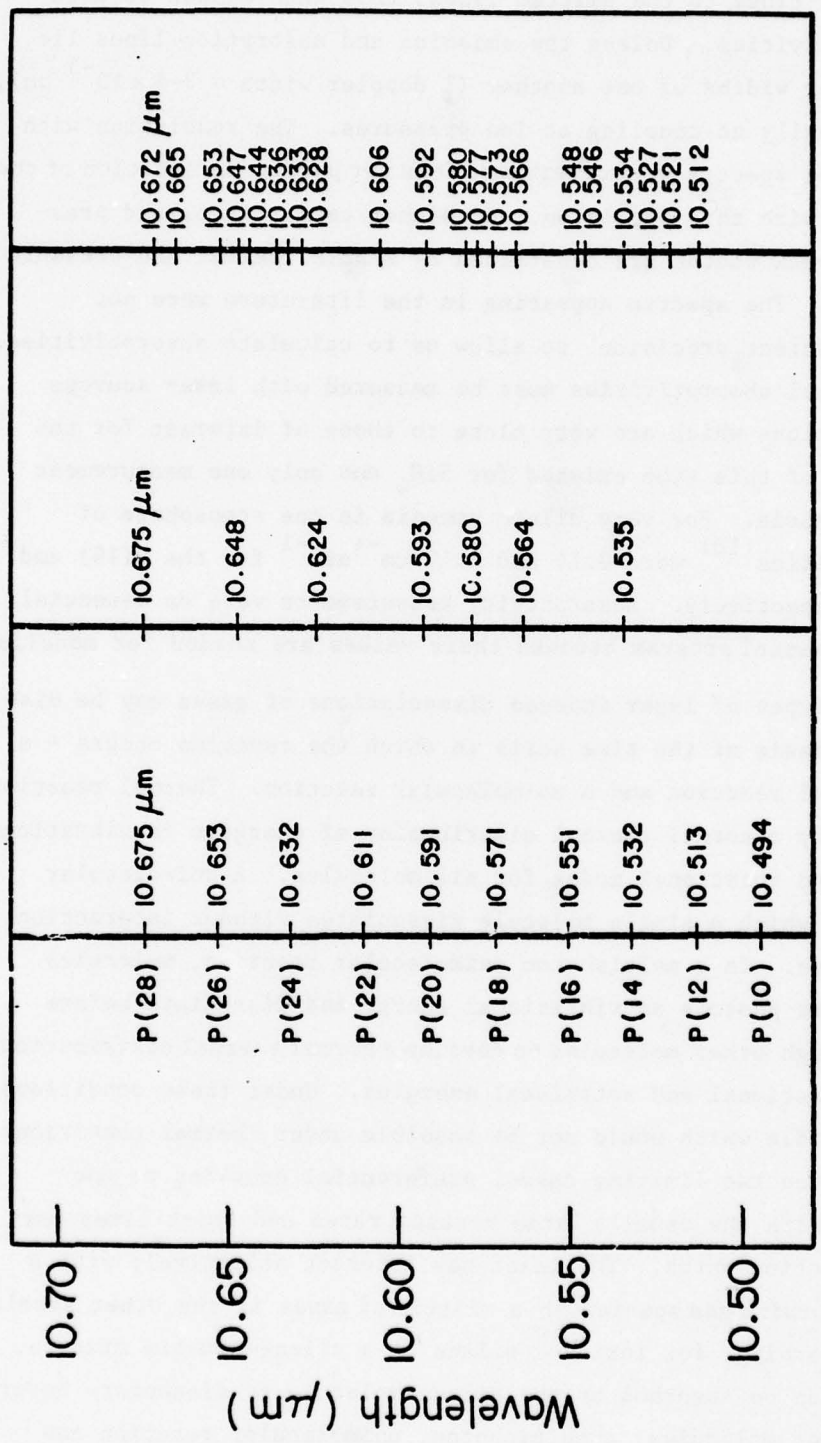

Figure 1. A comparison between the spectral absorption lines in SiH_3[8] and NH_3[9] near 10.6 μm, and the emission lines of a CO_2 laser.

be induced. If a large number of collisions occurs before dissociation, the silane acts as a heat source for the mixture and the reaction proceeds as a thermal one.

Unimolecular reactions have only recently been studied and it has been found that they are only possible at low pressure and extremely high intensity laser radiation. A sample calculation illustrates why this is true. A 10.6 μm photon has 0.1 eV energy and the average dissociation energy for an H atom from silane is 3.4 eV. Thus, at least 34 photons must be absorbed to cause dissociation. The energy transfer per collision is approximately 0.2 eV, so the molecule cannot suffer more than a few collisions while absorbing the exciting photons. At 10 Torr pressure, the reaction must occur in less than 10^{-7} sec, since the collision frequency is approximately 10^{8} sec^{-1}. With an absorption cross-section of $10^{-20}cm^{2}$, an intensity of approximately 10^{8} $watts/cm^{2}$ is required to transmit the dissociation energy/molecule in a 10^{-7} sec pulse. Higher intensities may not produce unimolecular reactions since the gas may break down into a plasma. In fact, only highly absorbing molecules are candidates for unimolecular reactions because of the breakdown phenomenon.

With laser intensities on the order of 10^{3} to 10^{4} $watts/cm^{2}$ and pressures near one atmosphere, the reactions can be expected to be well into the thermal region from the formal criteria of a normal energy distribution. The preferential coupling and the unusual time-temperature history may force the reaction from the normal path of a thermal reaction.

Based on the knowledge which was available at the initiation of the program, there appeared to be many exciting opportunities for using a laser heat source to produce improved Si_3N_4 and Si powders. The results of the first year's work indicate that these projections were valid.

B. Experimental Program

1. General Approach

Experiments have been conducted to develop quantitative descriptions of the absorption of energy emitted from a CO_2 laser by gas phase reactants and the response of the reactants to this type of heating. Ultimately, the results of these experiments will form the basis for a well understood synthesis process. Absorption and synthesis experiments have been conducted

in both static and flowing gas modes. Each of the synthesis experiments was carried out in two pieces of equipment. In total, five experimental configurations and two CO_2 lasers have been used.

The precise specification of cell pressure, temperature and optical path length which are possible in a static cell make this type of experiment best for absorption measurements. For synthesis however, static and flowing (dynamic) experiments each have specific advantages which makes both approaches useful.

The static synthesis experiments are a direct extension of the absorption experiments. Beam intensity, exposure time, and reactant partial pressures are manipulated to produce conditions which result in a reaction. These experiments permit a precise mapping of reaction thresholds which can be used as preliminary design data for flowing experiments and modeling analyses. The superior control of intensity, exposure time and the state functions of the reactants are extremely useful for studying the nucleation and growth rates. The extremes in peak power and pulse length, which are achievable with appropriate CO_2 lasers, permit possible unimolecular multiphoton reactions to be investigated in a more controllable manner in a static experimental configuration. The difficulty of collecting sufficient reaction products for characterization is the principal disadvantage of static experiments. Very small quantities of powders are produced and there are no means to force them to collect at convenient points within the cell. We also experienced an unanticipated, persistent problem of breaking laser entrance windows because powders formed on the windows where the most intense heating occurs.

Even though the process variables are not as precisely controllable in a flowing configuration, it is often more relevent to operate under steady state conditions than in a static, pulsed experiment. It's principal advantage is that large quantities of powders can be produced and the flowing gas transports the particles permitting them to be collected easily. A flowing experiment also simulates a production process which is obviously important.

2. Absorption Measurements

The absorptivity measurements were made in a manner which permitted the results to be interpreted directly in terms of the Beer-Lambert equation,

$$I = I_o e^{-\alpha p x}$$

where, I and I_o are the transmitted and initial laser intensities passing through a column of absorbing gas of depth x and at a pressure p. The pressure and temperature dependent absorptivity (α) is calculated directly from the experimental conditions and the observed I/I_o. The value of α is extremely sensitive to several factors which includes the exact wavelength of the emitted light, and both the temperature and pressure broadening effects that accompany absorption of light. While the theory is qualitatively useful, the quantitative measurements and their results must be viewed as largely empirical at this time. Therefore, experiments must be made very carefully over a range of conditions which approach, but do not exceed, the reaction thresholds. These absorptions measurements are based on a characterized emission from the laser.

a. Laser Emission

A Coherent Radiation Model 150 CO_2 laser was used for the absorption measurements since the majority of the synthesis work used this laser heat source. Other absorptions measurements which will be completed in the near future use a line tunable CO_2 laser.

The laser was tuned in the cw mode to emit a nominally gaussian energy distribution, which approximately coincides with the maximum emitted power. The laser's spectrum was analyzed in cw and pulsed modes with an Optical Engineering Spectrum Analyzer.

In a cw mode or in long duty cycle pulsed modes (pulse length $\geq$ 50% pulse period), this laser emits entirely at the P(20) line (10.591 μm). In a low duty cycle pulsed mode (pulse length $\leq$ 10% pulse period), the laser emits alternately on either the P(20), or the P(18) (10.571 μm) lines. The energy in individual pulses (measured with a Gen Teck joule meter coupled to a storage oscilloscope) was essentially constant (within ± 10%) whether the laser emitted on the P(20) or P(18) lines.

b. Absorption

The apparatus used for the absorption measurements is shown schematically in Fig. 2. The optical path length is 10.2 cm with the o-ring sealed KCl windows in place. The cell has ports which are used for gas inlet, evacuation and pressure monitoring purposes. Pressure is

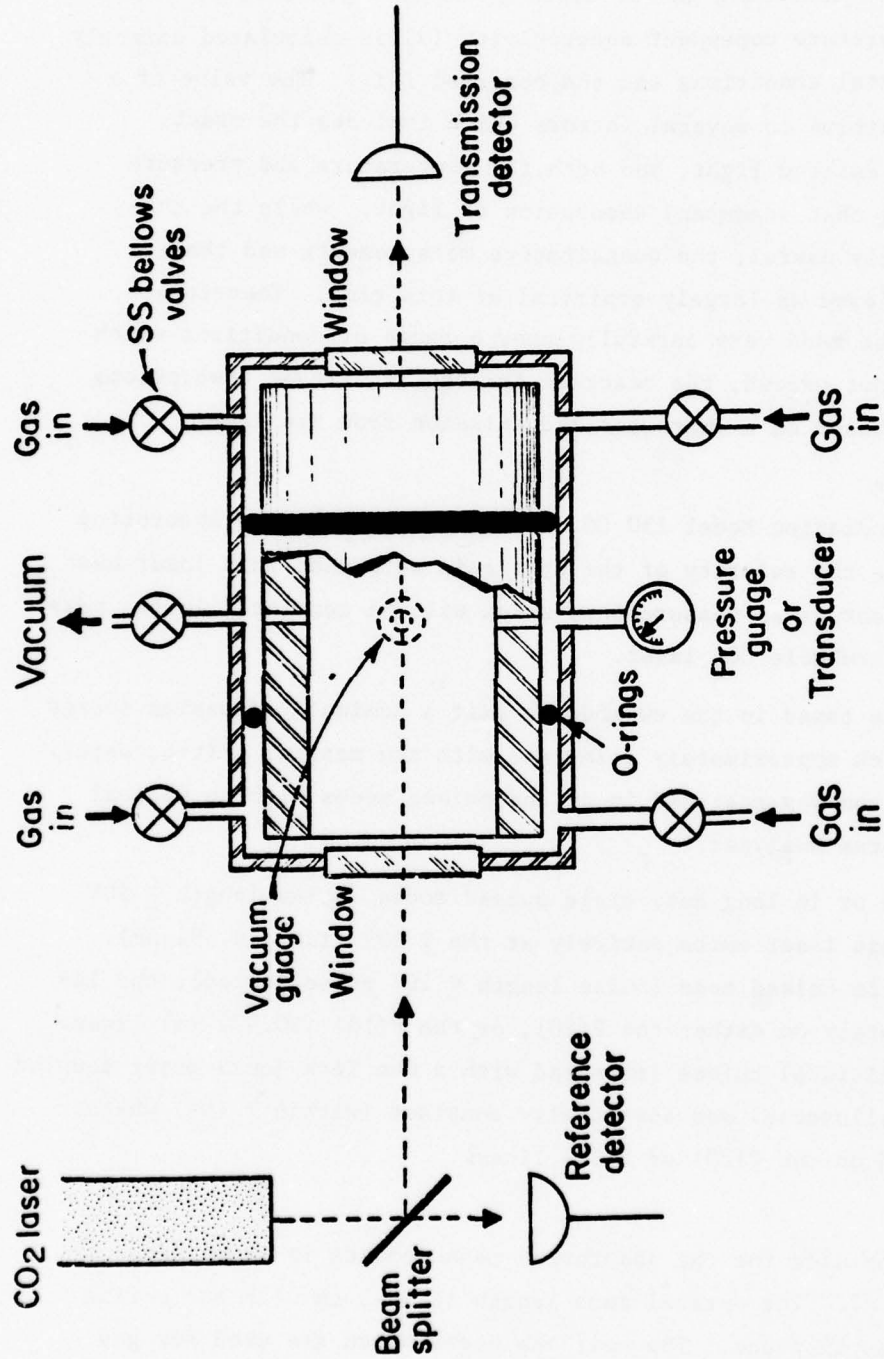

Figure 2. A schematic representation of the stainless steel cell used for absorption measurements and counterflow powder synthesis experiments. The inner sleeve and o-rings were removed for absorption measurements.

monitored during absorptivity measuremsnts to determine whether a reaction was induced since all of the reactions investigated produced a net increase in the number of gas molecules. Measurements were made under fixed volume conditions at predetermined initial gas pressures by alternatively measuring the pulse energy at the "transmission detector" either with or without partially absorbing gases in the cell. The ratio of these intensities yields the absorptivity directly since the effect of the absorptivities and reflections of the beam splitter and windows cancel out in the ratio. A KCl window was used as a beam splitter to reduce the pulse energy below reaction thresholds. The laser was pulsed at 1 hz with pulse lengths of 0.1 and 1.0 msec and energies of approximately 25 or 100 mJ.

The results of these measurements are shown in Figs. 3 and 4, which give the natural logs of the intensity ratios (equal to αpx) observed as a function of pressure for SiH_4 and NH_4 reactants. Figures 5 and 6 give the calculated absorptivities. Silane exhibited two distinct absorptivities which are attributed to the laser emitting on either the P(18) or P(20) line. The assignment of the lower absorptivity to the P(18) line was based on information from the literature[8] rather than direct correlation with spectrographic data. Ammonia exhibited equal absorptivities to the two CO_2 lines which are approximately 20 to 50 times lower than SiH_4 absorptivities.

The variation in silane's absorptivity with pressure is probably due to pressure broadening effects with closely spaced, strongly absorbing lines. With gas absorbers and laser emission sources, the apparent abosrptivity is a much more sensitive function of the overlap between an absorption line and an emission line than is apparent with conventional spectroscopy. At low pressures ($P \leq 1$ torr), the widths of the absorption lines and the laser emission lines are only approximately one doppler width ($\Delta\lambda \simeq 2\text{-}4 \times 10^{-5}$ μm). Unless the laser emission and gas absorption lines lie within a few doppler widths of each other, the absorptivity will be extremely low. The absorption lines broaden progressively with increasing pressure for pressure levels above a few torr. Since the total area under the absorption peak remains constant with increasing pressure, the maximum absorption intensity decreases as the peak broadens. The variation in apparent absorptivity with pressure will depend on both the relative locations of the emission and (possibly many active) absorption lines as well as the details of the broadening characteristics

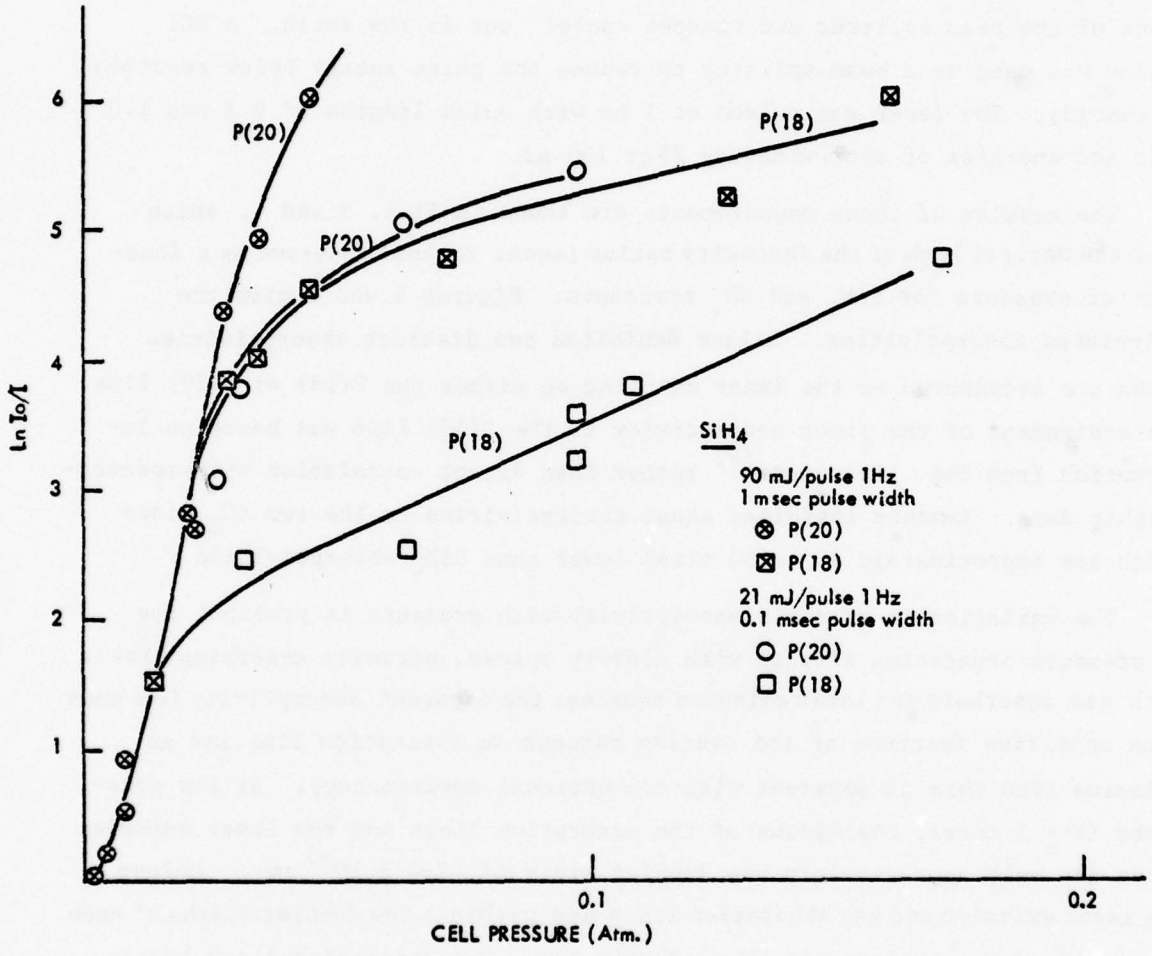

Figure 3. $Ln(I_o/I)$ versus cell pressure for SiH_4 at two different pulse intensities and two different emitting lines of the CO_2 laser.

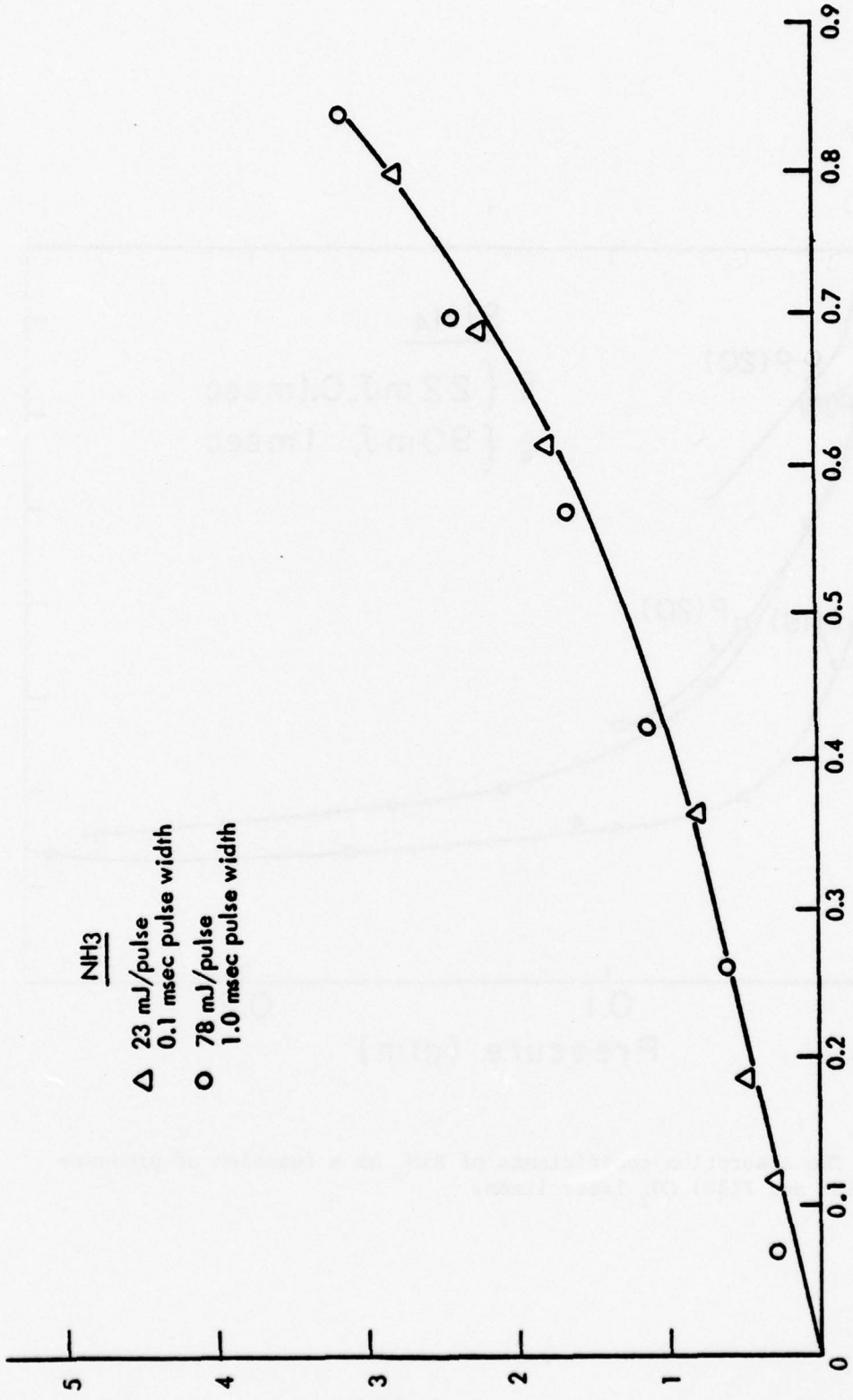

Figure 4. $\ln(I_o/I)$ versus cell pressure for NH_3 at two different pulse intensities.

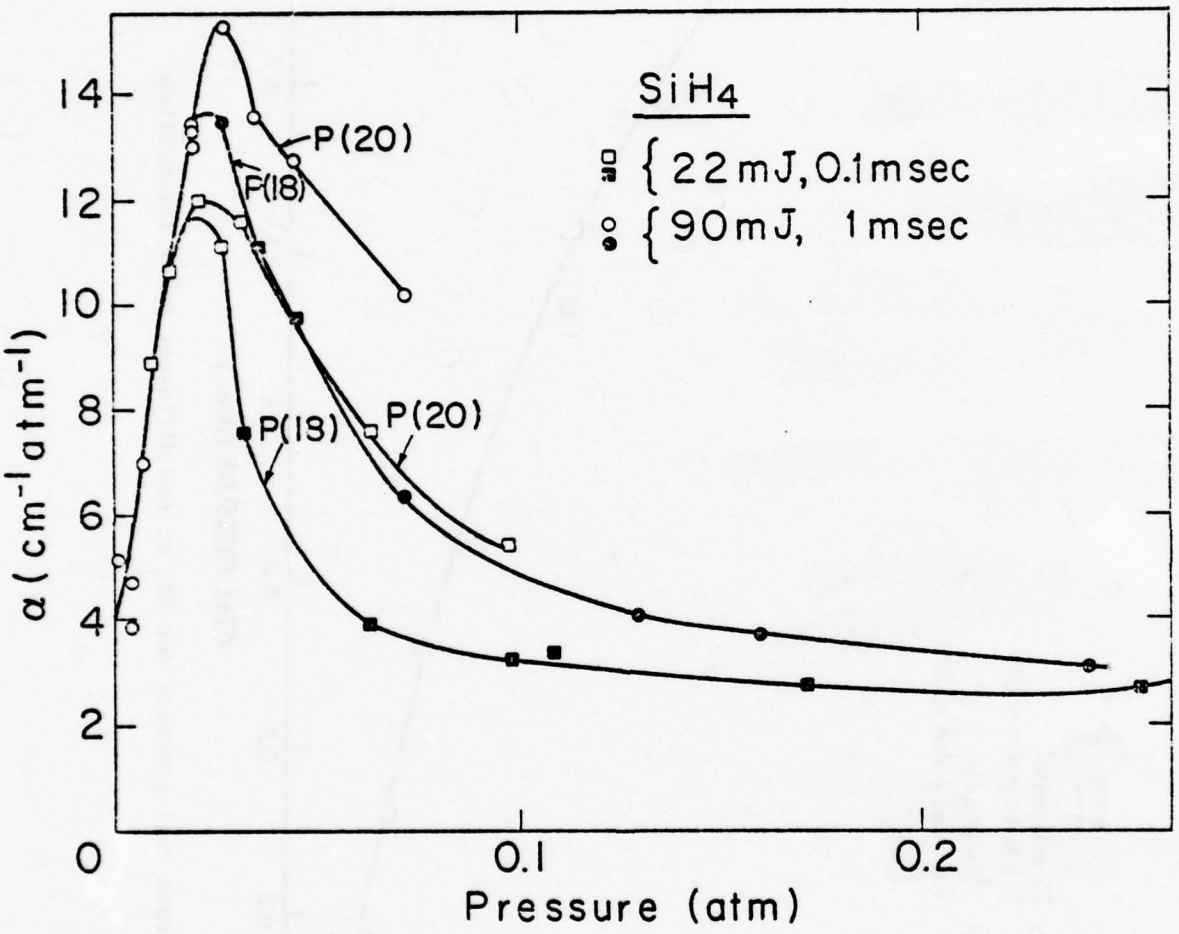

Figure 5. The absorption coefficients of SiH_4 as a function of pressure for the P(18) and P(20) CO_2 laser lines.

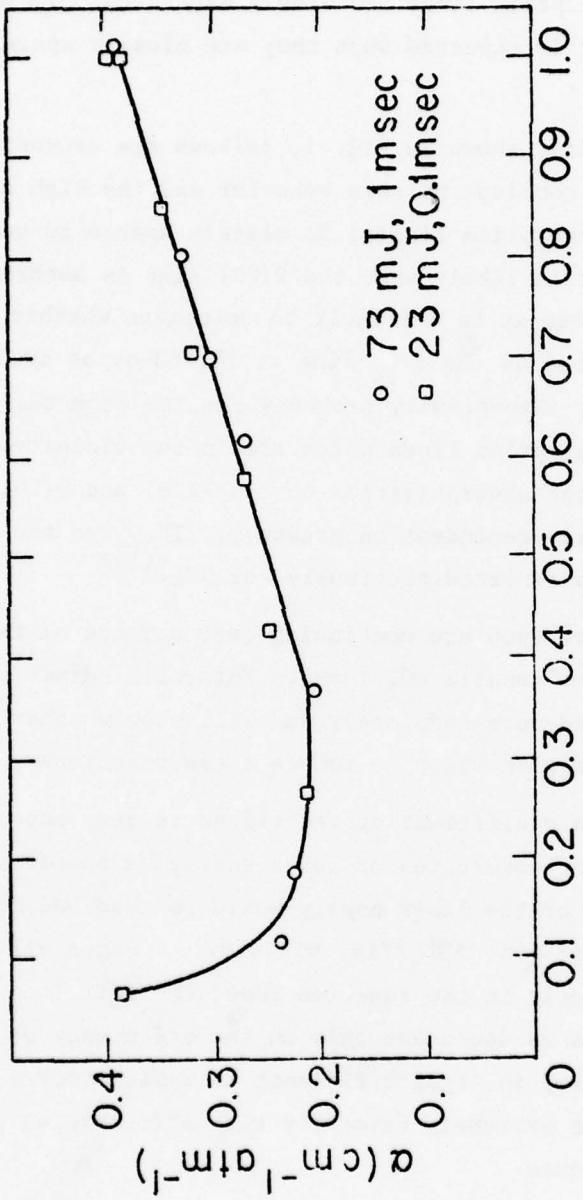

Figure 6. The absorption coefficients of NH_3 as a function of pressure for the P(18) and P(20) laser lines.

of each active absorption line. For a single absorption line, increasing pressures will cause an increased absorptivity as long as the peak broadening affects dominate and then may cause a decrease if the shrinking peak height affect dominates. A continuous increase in absorptivity is expected if the emission and absorption lines are widely separated. An ascending, then descending behavior is expected when they are closely spaced but are not coincident.

Silane's absorptivity, shown in Fig. 5, follows the ascending and descending pattern. We conclude by this behavior and the high absorptivities, that the active absorption line(s) is closely spaced to both the P(18) and the P(20) lines. It is likely that the P(20) line is absorbed by the SiH_4 line at 10.593 μm, but it is difficult to determine whether the P(18) line is primarily absorbed by the SiH_4 line at 10.580 or at 10.564 μm (see Fig. 1). Ammonia's absorptivity probably results from the combined effects of many weak absorption lines which are in the vicinity of the emission lines. Thus, the absorptivities to the P(18) and P(20) lines are equally low and weakly dependent on pressure. They are the same order of magnitude as has been reported previously for NH_3.[10]

Absorptivity measurements are continuing over a range of temperatures and pressures with a line tunable CO_2 laser. This will permit the absorption spectra to be interpreted more completely and will show whether there are more favorable emissions with which to induce these reactions.

The high absorption coefficient of the silane is very encouraging, since it allows efficient absorption of laser energy for powder synthesis. For instance, about 70% of the laser energy would be absorbed in the first cm of a one atmosphere of a 10/1 NH_3/SiH_4 mixture. Since all of the energy is absorbed directly in the reaction zone, the efficiency of the powder synthesis process is dependent only on the efficiency of the CO_2 laser. A 10-15% wall-plug to light efficiency is typical for a CO_2 laser. This efficiency compares extremely favorably with efficiencies of other powder synthesis techniques.

3. Powder Synthesis

a. Static-gas Synthesis

Two types of pulsed, static-gas experiments have been carried out. The first were used to map laser-intensity pulse-length thresholds required

to induce chemical reactions in SiH_4 and NH_3/SiH_4 mixtures. These experiments used the same laser and reaction cell as was used for the absorption experiments. They were intended to provide data for modeling studies and to serve as a design basis for continuous, flowing-gas synthesis. The second used a line tunable CO_2 laser which is capable of emitting substantially higher power pulses and shorter pulse lengths than the Coherent Radiation Model 150 used for the first type of experiments. In these experiments, the feasibility of inducing multiphoton, unimolecular reactions was investigated.

i. Reaction Thresholds

Reaction threshold experiments were initially undertaken in the cell shown in Fig. 2.

Threshold pulse lengths were determined for various reactant gas mixtures and pressures with fixed pulse intensities. The occurance of a reaction was detected by a permanent pressure change in the closed volume cell. Typically the transient pressure rise, which occurs with heating the gas, disappears within 30 msec unless a reaction occurred. Multiple pulses above threshold conditions caused visible concentrations of powder to form on the entrance window. The persistent formation of this powder caused us to abandon these static threshold determinations in favor of the flowing-gas experiments discussed in the next section.

It was anticipated that the powder deposit on the input window would cause two serious problems. Whether formed from SiH_4 or NH_3/SiH_4 mixtures, the powders would attenuate the laser beam resulting in erroneous, higher than actual threshold determinations, and also the KCl windows might be broken with large quantities of powder and high energy pulses. The only beneficial effect of powder forming on the KCl window was that the window could be used as a support for IR spectrographic analyses.

Static threshold and synthesis experiments, such as those reported in Table I, were successfully completed. They proved too time consuming to use for detailed mapping of the threshold conditions and were abandoned once it was verified that static and flowing experiments gave identical thresholds.

TABLE I. Experimental Conditions for the Synthesis of Several Powder Lots

Run Designation	Cell Pressure (Atmospheres)	NH_3/SiH_4 Flows (Std. cm^3/min)	Annular Flow (Std. cm^3/min)	Window Flow (Std. cm^3/min)	Laser Power (watts)	Pulse Length and Frequency or Exposure Times	Laser Mode
400 SN	.03 SiH_4 .03 NH_3	Static	-	-	15	-	cw
401 S	.05 SiH_4	Static	-	-	15	-	cw
402 SN	.053 SiH_4 .53 NH_3	Static	-	-	15	100 msec 1 hz	pulsed
200 S	.05	0/25	800	0	50	9.4 msec	cw
204 S	.50	0/16	900	84	135	14.7 msec	cw
205 SN	.20	40/11	400	600	50	4.6 msec	cw
207 SN	.20	110/11	400	600	150	1.9 msec	cw

ii. Unimolecular Reactions

To investigate the feasibility of inducing a unimolecular, multiple-photon process in silane, experiments were performed with a Tachisto TAC II Model 215G CO_2 TEA laser on samples of SiH_4 and NH_3/SiH_4 mixtures at pressures from less than 1 torr to 10 torr. The apparatus, shown schematically in Fig. 7, had already been utilized to investigate the laser induced dissociation of chlorinated ethylenes[11] and related compounds. The laser is capable of 0.5 J pulses with FWHM of about 50 ns and is line tunable over the 10.6 micron and 9.6 micron bands. The maximum peak power is approximately 10 megawatts. A two lens telescope focuses the beam inside the sample cell so that the beam intensity at the cell windows remains below the damage threshold but is sufficient at the focus to cause multiple photon absorption. Beam splitters monitor the incident and transmitted laser beam energy. The Pyrex (TM) cell, built especially for these experiments, is fitted with NaCl windows, an MKS 222A pressure transducer and a liquid nitrogen cold finger.

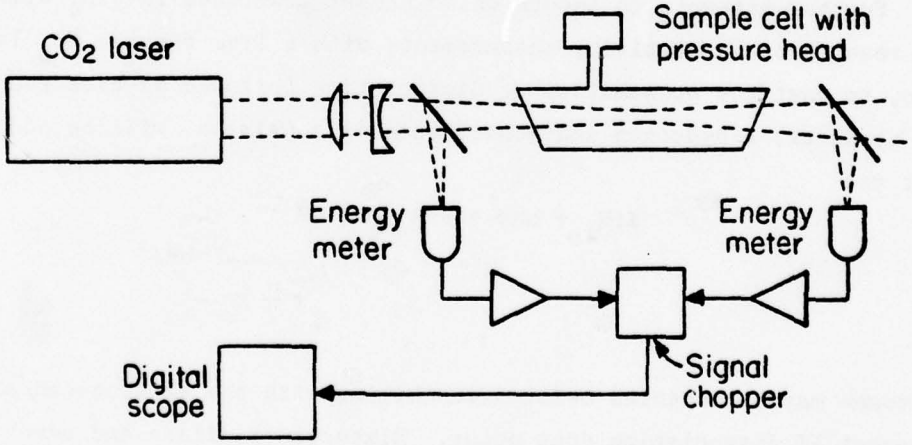

Figure 7. Schematic of laser, diagnostics and reaction cell used to investigate the feasibility of unimolecular reactions.

We have investigated the behavior of silane at pressures between 1 and 6 torr and peak fluences (I_p) between 12 and 190 J/cm^2,

$$I_p = E/\pi w_o^2 \quad ,$$

where E is the energy per pulse and w_o is the beam radius at the focus. These fluences correspond to peak intensities in the range of 24-380 megawatts/cm^2. Dissociation reactions were induced in these short duration, high intensity pulses. For instance, with an initial silane pressure of 5.4 torr, 27% of the sample was dissociated in 400 laser shots.

Although reactions were induced with P(20) and P(24) emissions, they do not appear to have resulted from multiple-photon absorption. Reactions occurred only when a white spark was evident near the focus of the beam. This is typical of, and is an indication that, dielectric breakdown occurred at these high fluences. Thus, the reactions were probably induced by plasma or arc heating rather than multiple-photon absorption.

In contrast with silane, SF_6 eliminates one F molecule and chloroethene eliminates HCl by multiple-photon dissociation processes of fluences of 1 J/cm^2 and 25 J/cm^2 respectively without dielectric breakdown. Both have higher absorptivities and can absorb sufficient energy to dissociate at intensities which do not exceed the thresholds for dielectric breakdown.

Further attempts to induce unimolecular reactions in SiH_4 will await the results of absorptivity measurements with a line tunable CO_2 laser. Also, to test the possibility of dissociation followed by back reaction of the products, a hydrogen scavenger, such as a halogen, will be added, so that via

$$SiH_4 + nh\nu \rightarrow SiH_{4-n} + nH \xrightarrow{+\frac{n}{2}X_2} nHX$$

hydrogen may be captured before recombining with the silicon-containing fragment if dissociation does occur. Mixtures of silane and ammonia will also be irradiated.

b. Flowing-gas Synthesis

Powders have been synthesized in a continuous manner directly from the gas phase in two reaction chambers. Both chambers were modifications of

equipment used for other experiments in this program. Most of the dynamic synthesis work was carried out under conditions where the beam axis and the gas-flow axis intersect orthogonally. This configuration permits the residence time in the beam to be characterized accurately and, if the gas stream is thin enough, the energy density within the beam is essentially constant. Flowing-gas synthesis experiments were also carried out in the cell used for absorption and static synthesis experiments. In this configuration, the beam and reactant gases travel in opposite directions along the same axis. These counter-flow experiments were initiated primarily to circumvent problems experienced in static threshold experiments with reaction products forming on the input window. This configuration is more efficient energetically than the orthogonal configuration, because all of the laser beam is eventually absorbed by the gas column. Also, all of the reactant gases can be subjected to the same thermal history while the intrinsic gradient along the axis of the laser beam in the orthogonal configuration will result in a varying history if the gas stream is optically thick.

i. *Orthogonal Geometry*

The cell used for these synthesis experiments is shown in Fig. 8. It was also used for particle size and shape modification experiments which are discussed in Section III.

The laser beam passes through the cell along a vertical axis. It enters via a hermetically sealed KCl window and is arrested within the cell by a water cooled copper block. Varying energy densities can be achieved by a combination of adjusting the laser power and the use of a lens positioned at various locations relative to its focal length. Most of these experiments used an unfocused beam (about 0.5 cm diameter) giving energy densities in the range of 60-800 watts/cm^2.

Reactant gases are injected into the laser beam by a 1 mm internal diameter stainless steel gas inlet tube. Either SiH_4 or premixed NH_3/SiH_4 mixtures (both undiluted) have been injected in this manner. A second gas inlet is used to surround the reactant gases with a flowing inert gas blanket which controls their expansion from the tip. Argon and nitrogen were used as the outer gas; NH_3/SiH_4 ratios were varied from 0-10.

Reactant particles were captured by means of a 0.1 μm diameter Millipore(TM) filter supported in a standard filter cartridge. A large fraction

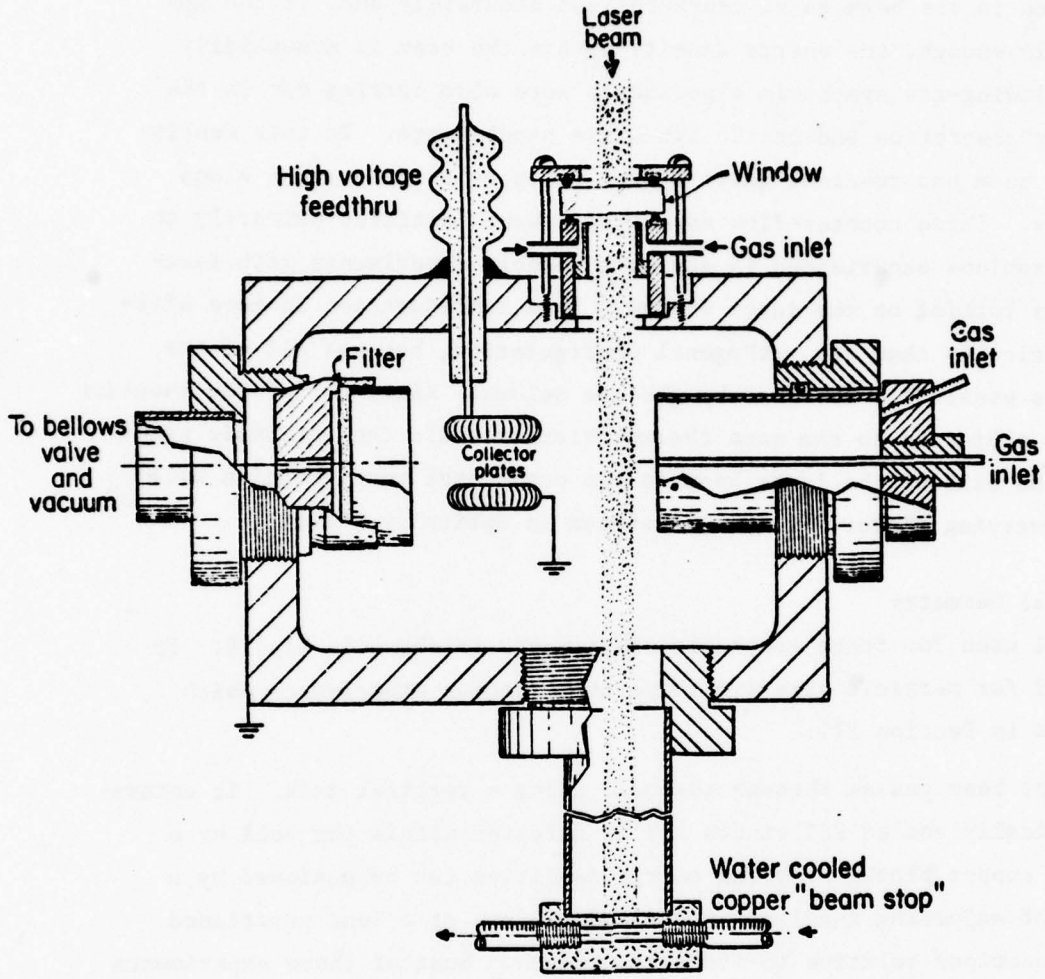

Figure 8. A cross-section of the reaction cell used for cross-flow experiments and particle comminution experiments.

of the particles remained entrained in the gas stream between the inlet tip and the filter and would build up as a low density cake on the filter. When the cake thickness exceeded 1 or 2 mm, the pressure drop across the filter became too high to control and the runs were terminated.

Single stage electrostatic collector plates were installed along the particle's path to determine whether particles formed with a net electrical charge of either sign. These experiments were also initiated before it had been demonstrated that the filter assembly could capture the particles efficiently. The static synthesis experiments produced particles with diameters in the range of 200-300 Å and filters with pore sizes in this range would not pass the required gas flow rates with acceptable pressure differentials.

After several modifications, the gas inlet adjacent to the laser window, shown in Fig. 8, successfully prevented particles from depositing on the laser window. As in the static experiments, these windows would crack if excessive accumulation was permitted. Typically argon was introduced at the window with a volumetric flow rate approximately equal to 6 times the reactants' flow rates.

Representative operating conditions for these experiments are shown in Table I. In general, gas flow rates and beam intensities were selected to have residence times which exceeded the reaction thresholds determined by pulsed experiments. Laser induced reactions of either SiH_4 or NH_3/SiH_4 mixtures were accompanied by an incandescent flame with roughly the same color, intensity and size as a burning match. The flame was evident at the first point of intersection between the reactant gases and the laser beam. The flame was lifted toward the top of the cell by bouyancy forces. Its rise was partially suppressed with higher reactant gas flow rates.

Under all investigated operating conditions, the powder product has been distributed approximately equally between the walls of the chamber and the filter. Most of the accumulation on the walls occurs on the chamber top in the trajectory of the flame. The remainder of the inner surfaces of the cell are coated with a thin layer of powder. The powder cake on the filter is relatively uniform in thickness. The density of the powder on the walls is much lower than that captured on the filter which is in the vicinity of 1% of theoretical.

The color of the powder depends on the NH_3/SiH_4 ratio and on the position within the cell. Pure silane reactant produces a powder which is light chocolate brown in color. Ammonia additions to silane result in an orderly distribution of colors ranging from pure white to light brown. The powder on the filter has a uniform light brown color and appears to be a homogeneous mixture of white and brown particles. At the top of the cell there is usually a smooth gradient from white at the thickest accumulation to light brown in the uniformly thin layer. Usually the lighter powder has a thin layer of brown powder underneath it at either the cell or the filter surface. The powder on other surfaces within the cell are tan to brown in color.

The application of maximum permissible electrical fields did not cause any major effect on the distribution of powders within the cell. At pressures in the vicinity of 0•5 atm., voltages in excess of 6 kV caused breakdown between the 1 cm spaced electrodes. Using either SiH_4 or NH_3/SiH_4 reactants, the application of an electric field causes a slight favoring of deposition on the top surface of the upper, negative electrode. Since the field strength between the grounded case and the negative electrode is the same order of mangitude as that between the two electrodes, this suggests that a small fraction of the particles may have a positive charge. They presumably remained on the top surface of the electrode because the mean gas velocity was lower there than between the two electrodes. Under the influence of a field, the particles formed from the SiH_4 reactant accumulated in stringers on the top surface of the negative electrode. These field effects suggest that the vast majority of the particles do not form with a charge of one sign and consequently a two-stage electrostatic precipitator would be required to capture these particles effectively. Contrary to this conclusion, it can be interpreted that the uniform distribution of particles on the cell walls results from their having like charges. Further experiments are required to clarify this issue.

Extended pyrolysis reactions have been performed in this cell using the conditions listed in Table I. Approximately three-fourths of a gram of powder was collected from lots 205 SN and 207 SN in runs which lasted approximately 45 minutes. Much more rapid rates of production are possible because, in these experiments, only a small fraction of the low power laser was absorbed by the small gas stream. The characteristics of resulting powders will be discussed in a later section.

ii. Counter-flow Geometry

Counter-flow synthesis experiments were carried out in the cell shown in Fig. 2. Slight modification was required from the configuration used in both the absorption measurements and the static synthesis experiments.

The stainless steel insert was put in place to direct the flow paths of the gas streams. Gases are pumped from the cell in a radial direction at approximately the midpoint along the cell's axis. An inert, transparent gas is introduced at the laser entrance window which flows axially along the beam's propagation direction. The absorbing reactant gases are introduced at the laser exit window. They flow axially, opposite to the beam's propagation direction. They meet the inert gas at approximately the midpoint in the cell where they are subjected to the full intensity of the laser beam and are then drawn out of the cell.

The principal advantage of this cell configuration is that the reaction occurs far away from the laser windows and reaction products do not reach the windows because of the gas flow directions. The inert gas protects the entrance window area and the beam is fully attenuated by the time it reaches the exit window, so there is no problem with heating in that region. The exit window can be used safely for direct observation or other optical characterizations of the reaction zone. An important feature of this configuration is that within the limits of the beam's and gas's flow uniformities, all of the reactant gases which intersect the laser beam are subjected to the identical laser intensity-time history. For laser pulse lengths which are short compared to the velocity of the gas, this experimental configuration is indistinguishable from a static synthesis experiment except for the important feature of preventing reaction products from forming on the windows. These features, combined with the good visibility of the reaction zone, proved to be a superior experiment for determining reaction thresholds than the static experiments.

Reactions were visibly evident in several ways. With long, high intensity pulses a weak, blood-red emission was evident near the center of the cell. Weaker or shorter pulses resulted in a momentary increase in the optical density of the gas within the cell; when sighting through the cell against a light background, laser intensity pulse-length combinations above certain threshold levels caused a darkening effect. Under some light com-

binations, wisps of white smoke-like powder were also visible. Threshold combinations were taken to be the minimum conditions which prcduced any visible effect. Thresholds determined in this manner agreed closely with the static thresholds identified by an irreversible pressure change.

The purpose of these experiments was to map the laser intensity pulse-length thresholds for reaction as a function of gas pressure and composition. The small quantities of powders which formed in pulsed experiments were not captured by any means. When cw experiments are initiated in the cell, a trap will be installed in the gas exit line. The results of the reaction threshold experiments with SiH_4 and NH_3/SiH_4 mixtures are shown in Figs. 9 and 10.

These experimental results are reported separately on Figs. 9 and 10, because the laser pulse characteristics change for pulse lengths shorter than approximately 10 msec. For pulse lengths longer than approximately 10 msec and laser beam plasma current in the range of 20-50 ma, the intensity of the laser beam is independent of pulse length. Thus, the energy emitted in a pulse is directly proportional to pulse length. For pulse lengths shorter than 10 msec, the average beam intensity in this particular laser becomes dependent on pulse length. Fig. 10 indicates the average pulse intensity as a function of pulse length. The longer pulse length experiments employed a KCl beam splitter to reduce the intensity of the beam at the cell to approximately 10% of the emitted beam.

C. Analysis

1. Powder Characterization

Resulting powders have been characterized by techniques which reveal the size, shape and specific surface area of the particles, their crystal structure, the chemical constituents and the bonding. Transmission electron microscopy (TEM), scanning electron microscopy (SEM) and scanning-transmission electron microscopy (STEM) instruments have been used for direct observation and chemical characterizations. BET measurements were used to evaluate specific surface area. Infrared spectroscopy and wet chemical analyses were used to determine stoichiometry and purity. Debye-Scherrer x-ray, and electron diffraction techniques were used to determine whether the powders were crystalline.

Results indicate that the characteristics of the particles depend primarily on the specific reactants which were present and not on whether

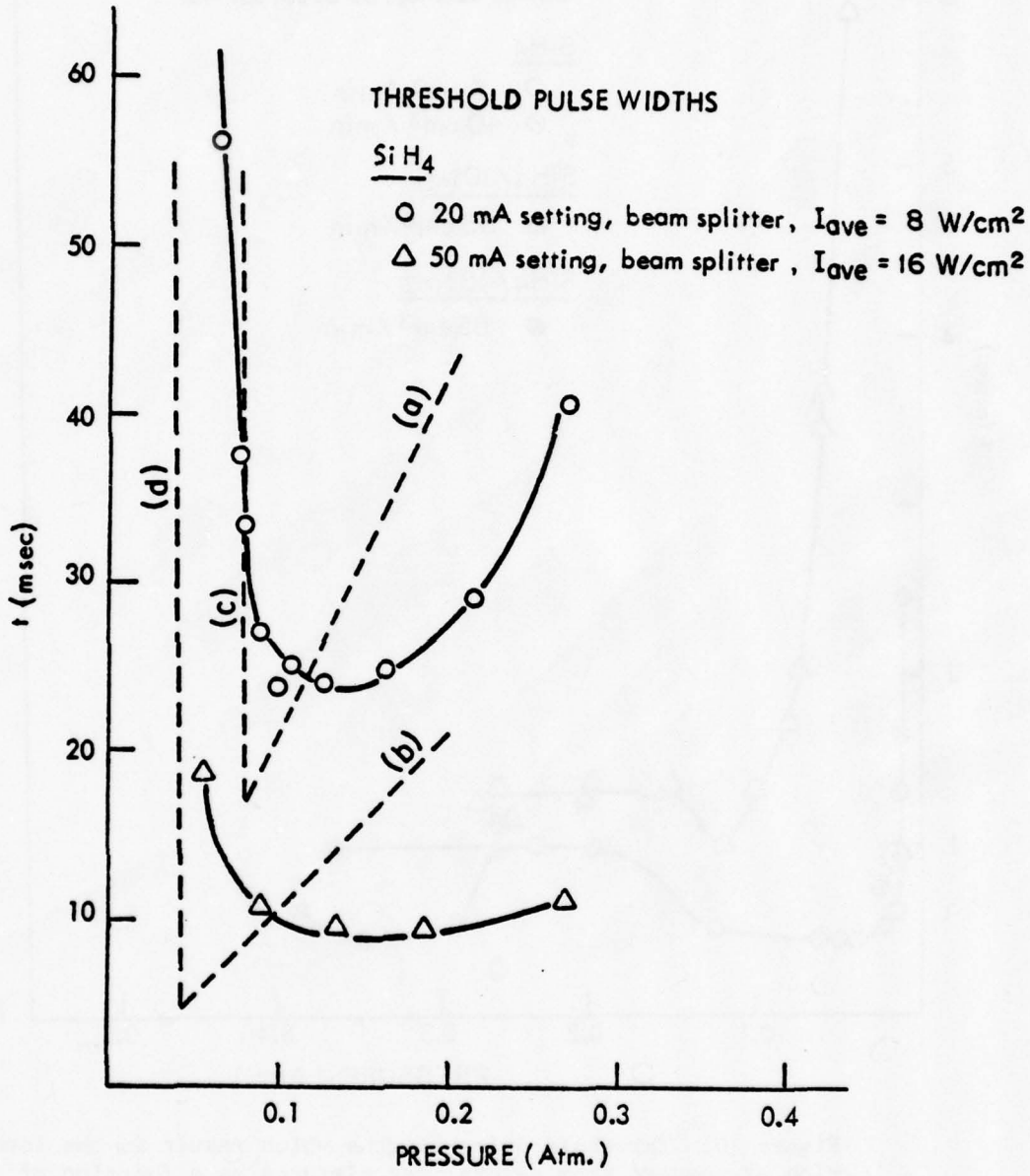

Figure 9. Threshold pulse-lengths which result in the formation of Si powder from SiH_4 as a function of pressure. Dotted lines a, b, c, and d are calculated thresholds equating the absorbed power to the sensible heat (a,c) and to the conductive losses (b,d). Lines a and c correspond to 8 w/cm^2 and b and d correspond to 16 w/cm^2.

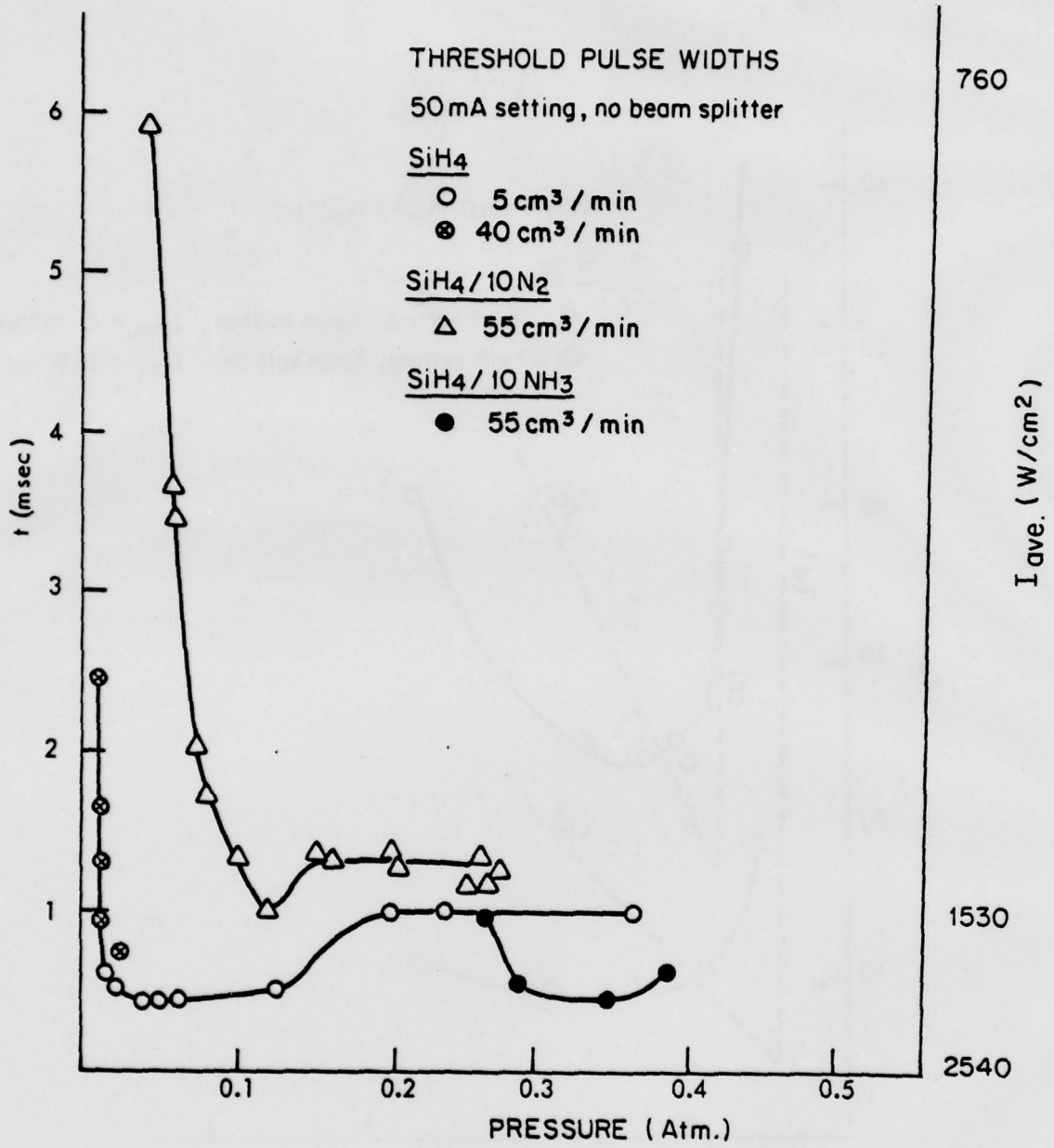

Figure 10. Threshold pulse-lengths which result in the formation of powders from several gas mixtures as a function of pressure. Pulse length dependent pulse intensities are indicated. For pulse lengths greater than 10 msec, I_{ave} equals 760 watt/cm^2.

the experiment was static, flowing, pulsed or cw. At present, we have observed that smaller particles are produced with shorter exposures to more intense laser illumination. More detailed characterizations may reveal other correlations in the future.

a. Physical Characteristics

The particles produced by laser pyrolysis are unusual with respect to powders produced by conventional processes. Their diameters are smaller, they have a narrower size distribution, and they are equiaxed. Photomicrographs of representative powders are shown in Figs. 11 through 13. We have not investigated the nature of the interparticle bonds in these clusters. Typically particles formed from dilute gas phase reactions are weakly bonded because the particles grow from widely separated nuclei and there is no neck growth between them.

Based on a limited number of experimental conditions and characterizations, it appears that increased laser power intensity, higher NH_3/SiH_4 ratios and lower reactant pressures produce a more uniform particle size distribution. The most uniform distributions observed were produced at the highest NH_3/SiH_4 ratio (10/1) and the highest power intensity. Specifically, run 207 SN (Table I) which is typical of our later and more controlled silicon nitride runs, produced particles which were all between 100 and 200 Å in diameter. Simultaneously reducing the power and the NH_3/SiH_4 ratio (run 205 SN) resulted in particles that were mostly between 100 and 400 Å in diameter; but a few particles between 400 and 1000 Å in diameter were evident. Particles resulting from pyrolysis of SiH_4 were generally in the ranges of 200-600 Å to 200-1000 Å in diameter depending on conditions.

It is apparent that in most cases, many experimental parameters were varied simultaneously in these experiments, so it is not possible to definitively attribute and quantify a cause-and-effect relationship to the process variables which determine particle diameters. Systematic experiments are in progress which will isolate and determine these effects.

It is also apparent that even with widely varying non-optimized process conditions, small, relatively uniform diameter particles are produced by the laser heated process. No other process of which we are aware has demonstrated a capability of producing Si_3N_4 powders with particles which are all between 100 and 200 Å (116 m^2/g). In terms of the criteria stated for an ideal powder, the best reported results were achieved by Prochazka and Greskovich.[2]

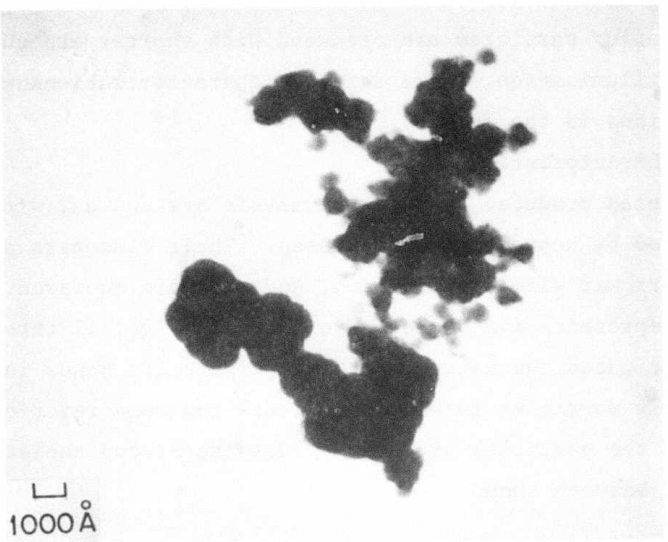

(a)

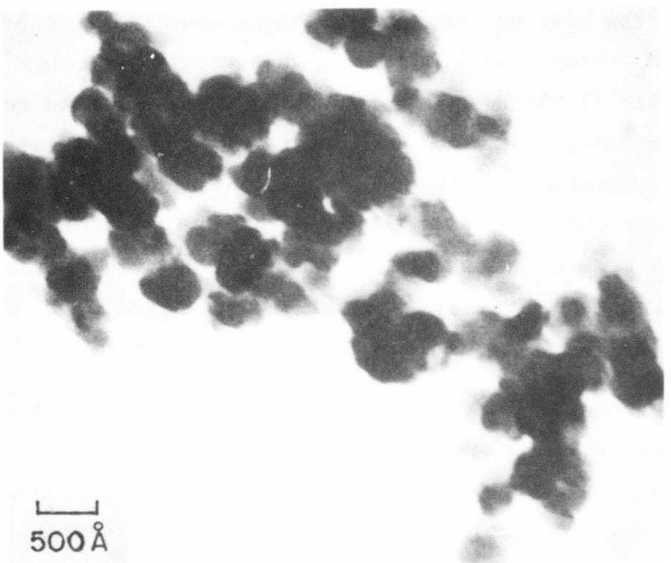

(b)

Figure 11. STEM micrographs of powders.
(a) 400 S and (b) 401 SN.

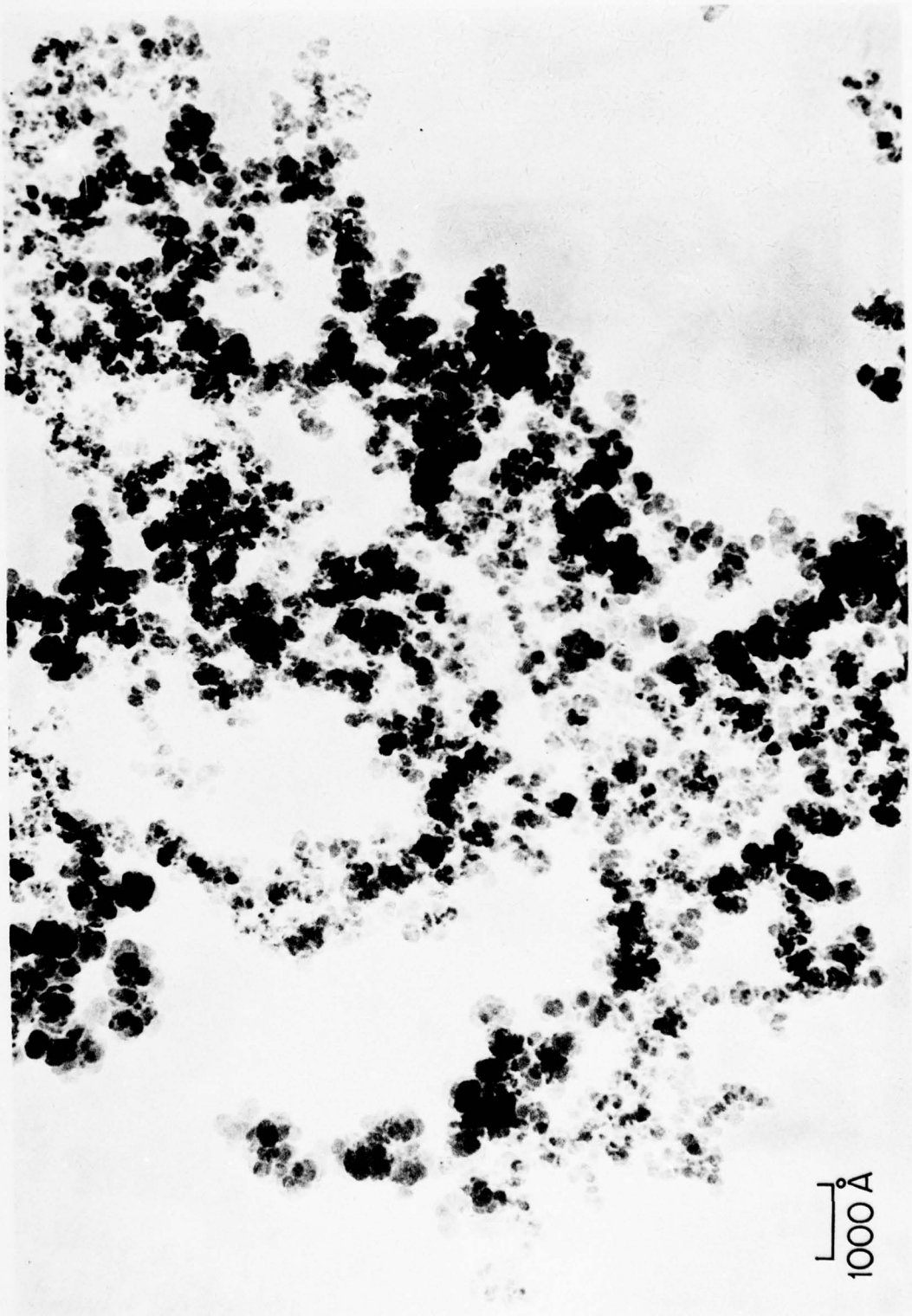

Figure 12. TEM micrograph of Si powder 200 S made from SiH_4.

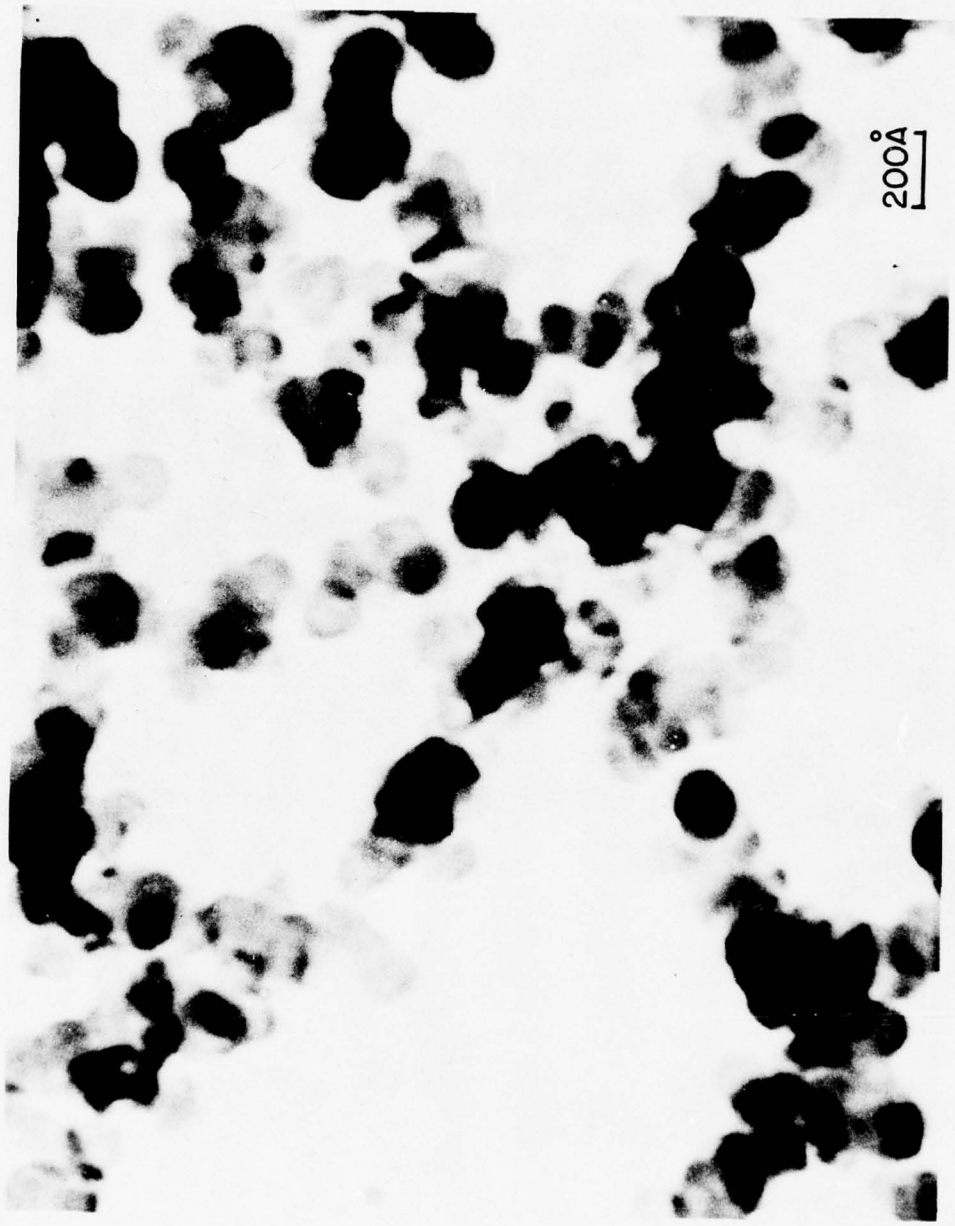

Figure 13. TEM micrograph of Si_3N_4 powder 012 SN made from $10NH_3/SiH_4$.

reported typical particle sizes in the range of 300-2000 Å; under specific conditions they achieved powders (80 m^2/g) with somewhat smaller diameters. The lack of extreme sensitivity to laser process variables is an important characteristic from the standpoint of developing a controllable manufacturing process. Major excursions in processing conditions will probably permit an orderly manipulation of particle sizes which is exemplified by the high peak intensities (about 10^9 w/cm^2) and short pulse lengths (10^{-9} sec) used in our attempts to induce unimolecular reactions that produced powders with diameters in the range of 25-50 Å.

Specific surface area measurements, made by the BET technique, are given in Table II. The spherical diameter which is equivalent to the specific surface area agrees with the direct TEM diameter measurements. In the case of powders 200 S and 205 SN, only a very few particles were observed beyond the 200-600 Å range, so the agreement between the two techniques is better than is apparent from Table II. This equality between the two diameters indicates that the particles do not have open porosity and have smooth surfaces. Particle densities have not been measured yet.

TABLE II. Results of BET Specific Surface Area Measurements

Powder Identification	Specific Surface Area	Equivalent Spherical Diameter*	Diameter from TEM
200 S	97 m^2/g	193 Å	100-500 Å
205 SN	82 m^2/g	228 Å	100-1000 Å
207 SN	116 m^2/g	161 Å	100-200 Å

* Assuming $\rho = 3.2$ g/cm^3

b. Crystal Structure

Powders have been analyzed by x-ray diffraction and selected area diffraction techniques (TEM and STEM) to determine whether the particles are crystalline, and if so, to identify their crystal structure.

X-ray diffraction patterns were made by the Debye-Scherrer technique using Cu Kα radiation. Approximately 16 hour exposures were required. Representative diffraction patterns are shown in Fig. 14 for powders produced from SiH_4 and NH_3/SiH_4 mixtures.

Powders produced from SiH_4, which are brown, (Fig. 14a) yield two broad diffraction peaks. The inner peak includes the most intense (100%) Si(111) peak. The outer peak includes the 60% Si(220) and 35% Si(311) peaks. Powders synthesized from NH_3/SiH_4 mixtures which are white to light tan in color yield one very broad peak (Fig. 14b). This broad peak includes the most intense peaks from both α and β polymorphs of Si_3N_4; i.e., α(100), (210) and (102) and β(200) and (201). The dark tan to brown powders produced from NH_3/SiH_4 mixtures yielded the same diffraction pattern as the white powders. It is yet to be determined whether color is a reliable indication of powder chemistry.

The extreme line broadening prevents the identification of the nitride phase which formed. The apparent line broadening exceeds that which would be expected for 200-300 Å diameter particles. Using the expression[12]

$$d = \frac{0.9\lambda}{B \cos \Theta_B}$$

where d is the particle diameter, λ is the wavelength, B is the peak breadth at 1/2 intensity and Θ_B is the Bragg diffraction angle in radians, to calculate a particle size corresponding to the observed peak breadths, yields Si diameters of approximately 20 Å. The discrepency between the calculated and observed diameters could result from the following factors. Particularly with Si_3N_4, the apparent B is probably much larger than the actual values, since the observed peaks likely result from several overlapping broadened peaks. The crystal structure may be highly distorted to amorphous and/or the particles may be extremely fine grain polycrystals. X-ray characterization is continuing in conjunction with annealing studies to provide a better description of these powders.

There are only preliminary electron diffraction results. Powder 207 SN produced a ring pattern which is distinctly different from the amorphous carbon grids, but this does not give definitive evidence of crystallinity. Dark field and lattice imaging techniques will be used to determine whether the particles are crystalline.

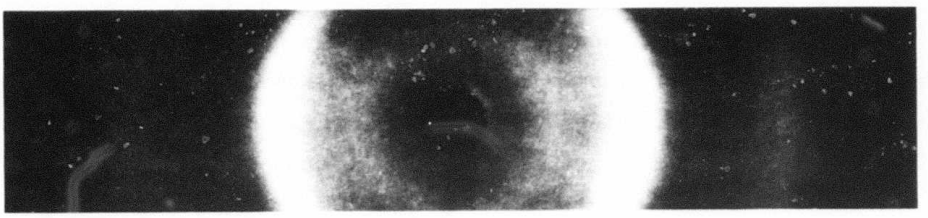

(a)

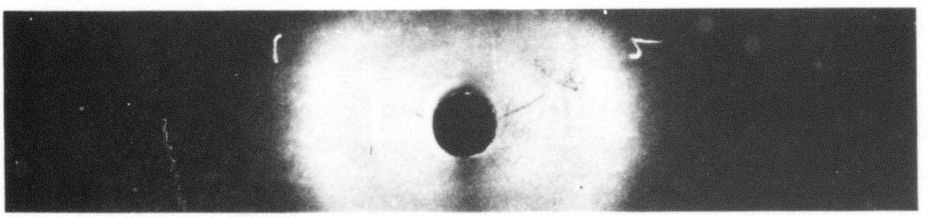

(b)

Figure 14. Debye-Scherrer x-ray diffraction patterns of powders (a) 401 S and (b) 400 SN. Exposure conditions: 15mA, 35 KV and 16 hours.

Although these x-ray results have some ambiguities, the diffraction results indicate that the powders have some crystalline characteristics. They also demonstrate that either Si or Si_3N_4 powders can be produced from appropriate reactants.

c. IR Spectrometry

Spectrographic analyses have been made of powders produced by both static and flowing gas techniques. Figure 15 shows spectra of powders produced under static conditions from SiH_4 as well as NH_3/SiH_4 reactants. In this case the spectra were taken from powders supported on the KCl cell window. Figure 16 shows powder spectra produced from flowing NH_3/SiH_4 mixtures as well as an amorphous Si_3N_4 powder which is commercially available (Sylvania SN 402). These powders were mixed with KBr and pressed into a pellet at 15,000 psi (2×10^{-3} gr powder per gr KBr). The spectra on Figs. 15 and 16 appear somewhat different from one another because they were taken on different instruments which produced the data on different scales.

These spectra exhibit a number of identifiable characteristics. The short wavelength cut off below nominally 3 μm results from the band gap in free Si. These absorption peaks have the following identities:

Wavelength (μm)	Bond
3.0	possibly N-H or O-H
4.6	Si-H
6.1	O-H
7.2	unknown
9.0	Si-O
11.5	Si-N
21.0	either Si-N or Si-O

The absence of the 21.0 μm peak in Fig. 15 is caused by masking from KCl windows used to support the powders. Figure 15 illustrates the disappearance of free Si with the addition of NH_3 to the SiH_4 reactant. Figure 16 shows no evidence of free Si in these three powders. All of the powders indicate the presence of oxygen, but we have not determined whether this element is introduced during synthesis or during subsequent exposure to air. Either

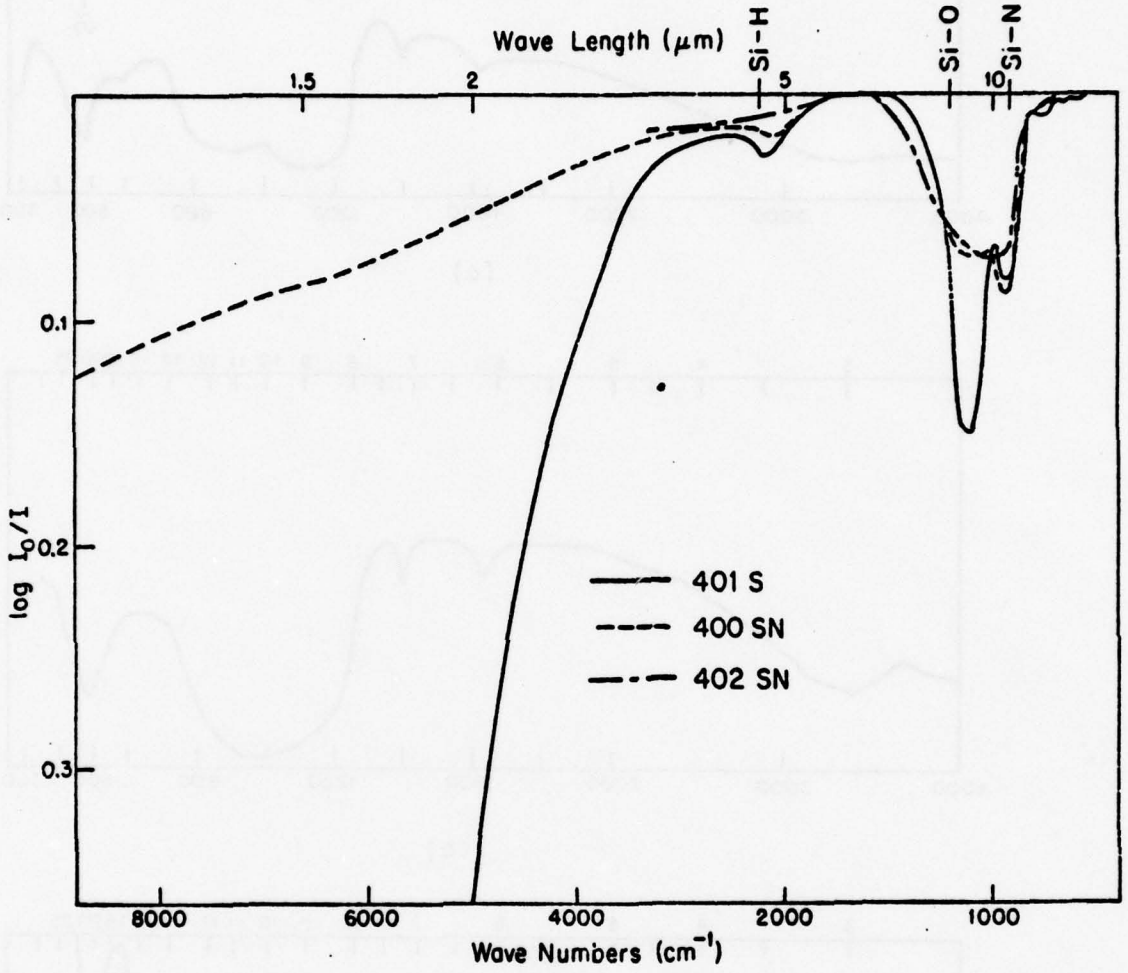

Figure 15. Infrared spectra between 1 μm and 20 μm of powders: (a) 401 S, (b) 400 SN and (c) 402 SN.

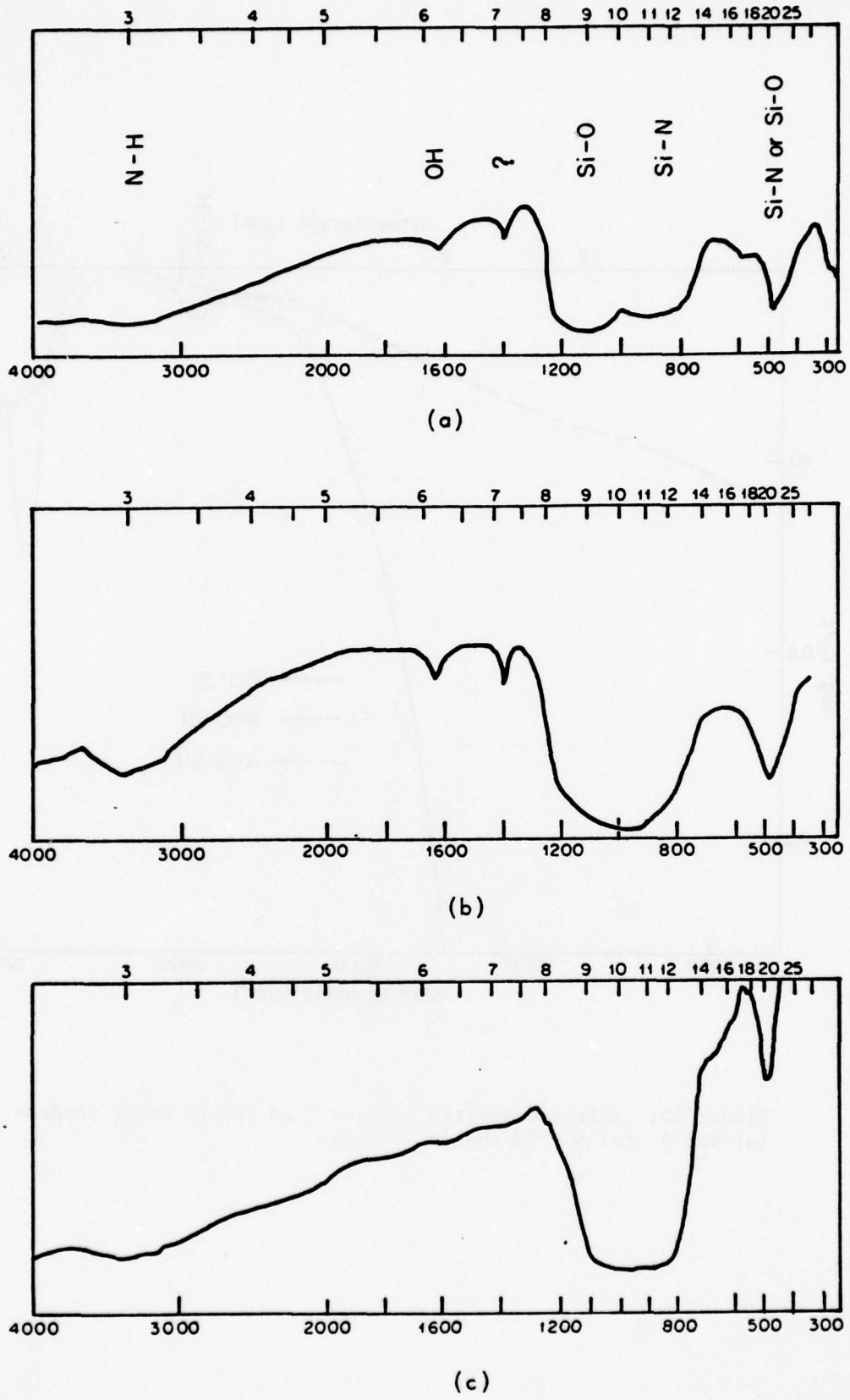

Figure 16. Infrared spectra between 2.5 μm and 25 μm of powders: (a) 205 SN (b) 207 SN and (c) Sylvania SN 402.

an absorbed layer or a reaction layer which is a few monolayers thick constitutes approximately 10% of the volume of a 300 Å particle. Particularly with the strong Si-O absorption peak, spectral features arising from surface effects might be observable superimposed on the bulk spectral features. Based on systematic studies[13] of the effects O_2 and N_2 have on shape and location of the Si-N and Si-O peaks, we have tentatively concluded that oxygen is present within the bulk of these particles and is attributable to some combination of impurities in the reactant gases or atmospheric leaks. In either case, oxygen contaminations can be eliminated in a straight-forward manner. The results shown in Fig. 15 show that increasing NH_3 concentrations reduce the intensity of the Si-H peak. The nitrogen apparently displaces the H_2 from the solid. Figure 16 shows that powders made by the laser process have the same major features as Sylvania (SN 402) Si_3N_4 powder.

These results support the principal conclusion made from x-ray analyses; that either Si or Si_3N_4 powders can be made by the laser heating process. The lack of fine structure between 10 and 20 μm in the IR spectra tend to indicate an amorphous powder. Work is continuing to improve the understanding of the IR spectra. The interaction between the Si-N and Si-O absorption bands makes quantitative interpretation of some spectral features very complex.

d. Chemical

Because of the small quantities of powders which were produced until very recently, quantitative wet chemical analyses were not possible. EDX analysis on the STEM revealed only Si for several powders synthesized from static gases. These showed that there were no contaminants with atomic weights higher than 13. One set of 4 samples has recently been analyzed by wet chemical analysis for Si, N_2, H_2 and O_2. These results are given in Table III.

TABLE III. Results of Wet Chemical Elemental Analyses

Sample	Oxygen %	Hydrogen %	Nitrogen%	Silicon %
A	0.48	0.031	37.3	58.0
B	0.47	0.15	0.025	99.0
C	3.07	0.458	12.8, 14.7, 14.8	58.0
D	.40	0.477	36.2	59.2

Samples A and D were taken from the same powder (KBI CP85) for purposes of determining the reproducibility of the analyses. Sample B was synthesized from flowing SiH_4 and Sample C from flowing 10/1 NH_3/SiH_4 mixture. The weight percentages nitrogen and silicon in stoichiometric Si_3N_4 are 40 and 60 respectively.

It appears that the analyses for all elements are reproducible to approximately one per cent by weight. With the exception of sample C, the total of all elements are in the range of 95-99% which also indicates an accuracy of approximately ± 1%. Within this precision, these individual analyses also agree with the values expected for Si_3N_4 and Si. The two anomalies are the nitrogen content in sample C and the oxygen contents.

As indicated in Table III, the nitrogen analysis was made three times for sample C. In each case the determined nitrogen content was approximately 1/3 the value expected for stoichiometric Si_3N_4. We feel that the problem with the analyses probably lies with the indicated nitrogen content rather than silicon, and is caused by the unusually small particle size.

The oxygen contents indicated in samples A and D are substantially lower than expected from both KBI's analysis (about 1.8%) as well as general experience with commercial Si_3N_4. Chemical analysis, as well as IR spectrographic analyses, indicate the presence of oxygen in samples synthesized with laser heating, which is not surprising considering that these samples were allowed to sit in air for long periods of time, but as mentioned in the previous section the oxygen may be bulk oxygen introduced during synthesis as well. A glove box is being installed so that samples can be prepared and analyzed without exposing them to air in order to better understand the origin of the oxygen content.

Hydrogen analyses indicate that very little hydrogen is trapped and/or incorporated in solids.

While these chemical analyses do not confirm the synthesis of stoichiometric Si_3N_4 powders, the results do not preclude this possibility. The silicon content found in sample C is almost precisely the value expected for Si_3N_4. Any significant departure of stoichiometry toward the nitrogen deficient side, should probably have revealed IR absorption characteristics of free

silicon. Since this was not observed, we conclude that the nitrogen content is erroneous.

2. Thermal Analysis

The equation which describes the absorption of laser energy and the resulting temperature rise and heat losses is straight-forward to write, but has not been solved in a general manner. The solution is difficult because optical characteristics of the materials are not well known and mass/heat transfer processes are intrinsically difficult. Limiting solutions have been developed.

The heat power balance in any volume element of partially absorbing gas exposed to light is given by the following equation:

$$I_o \Delta A \exp(-\Sigma \alpha_i p_i x)[1 - \exp(-\Sigma \alpha_i p_i \Delta x)] = C_p \frac{n}{V} \Delta V \frac{dT}{dt} + \Delta H \Delta V \frac{dn}{dt} + \text{heat transfer losses}$$

where: I_o is input intensity in watts/cm^2

ΔV is the element of volume in question

ΔA is the cross section of the element ΔV

α_i is the absorption coefficient of the i^{th} species

p_i is the partial pressure of the i^{th} species

x is the distance of the element ΔV from the window

Δx is the thickness of the element ΔV

C_p is the heat capacity of the gas

$\frac{n}{v}$ is the molar density in the volume element ΔV

$\frac{dT}{dt}$ is the rate of change of temperature

ΔH is the heat of reaction in joules/mole

$\frac{dn}{dt}$ is the moles of gas reacting per unit of time per unit volume.

The geometrical relationships are shown in Fig. 17. The expression on the left of the equation indicates the heat dissipated within a volume element ΔV after a beam, having an initial intensity I_o, has traveled a distance x through a partially absorbing medium. The terms on the right represent the means by which the absorbed heat can be dissapated. These are the sensible heat, the latent heat, and heat losses by conductive, convective and radiative processes.

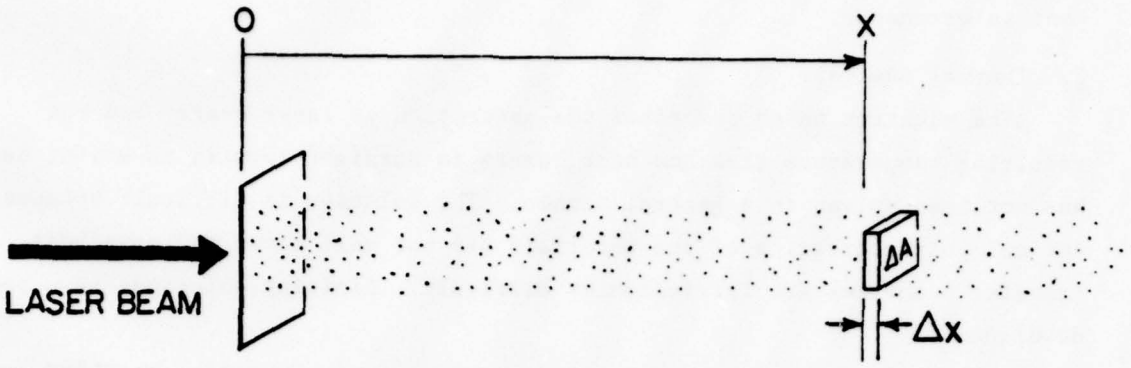

Figure 17. Schematic representation of the volume element, ΔV, within a column of gas which is absorbing the laser beam. At $x \leq 0$, there is no absorption of the laser beam.

The details of the absorption expressions become uncertain once sufficient power has been absorbed to cause heating along the path of the beam. Sudden temperature rises cause both the α_i and the p_i values to change. The experimental results shown previously in Figs. 5 and 6 show how α_i varies with moderate pressure changes under essentially constant temperature conditions. It can be anticipated that the α_i's will vary with temperature, but no experimental measurements have been made yet. Also, no α_i measurements have been made through partially or completely reacted gases. These factors, combined with the uncertainties about the temperature, pressure and density along the path of the laser beam preclude meaningful calculations for locations which are remote from the first interaction volume. To evaluate the terms on the right, it is necessary to develop a model for mass transfer which accompanies the intense localized heating from the laser as well as that from the exothermic reactions. We are presently developing models and evaluating the solutions. To date, only simplified solutions have been examined to explain the high and low pressure regimes of the threshold experiments shown in Figs. 9 and 10.

One set of solutions considers the volume element which is first exposed to the laser beam. In the counter flow geometry, this is at the plane where the two axially flowing gas streams intersect. This point is subjected to the most intense illumination within the cell, consequently it is the first to reach threshold conditions. Also, the illumination intensity is not complicated by a complex "upstream" history. For this set of solutions, we have assumed that the reaction proceeds spontaneously to completion when the

premixed reactant gases reach a critical temperature. The exothermic heat, therefore, does not affect the threshold. Convective and radiative heat losses were assumed to be negligible. The assumption about convective heat losses is valid since the pulse lengths are short compared to the gas residence time in the cell. Below threshold temperatures, the radiative power of the gas is very low. Conductive heat loses are considered below.

The first solution assumes that all of the absorbed heat is converted to sensible heat. Using the substitutions $\exp(-\alpha p \Delta x) \simeq 1 - \alpha p \Delta x$ and $\frac{n}{V} = \frac{P}{RT}$, and a correction for the effect of temperature on absorption ($\overline{\alpha p}(T) = \alpha_o p_o \frac{T_o}{T}$) with constant pressure gives

$$\Delta t = \frac{C_p (T_R - T_o)}{\alpha_o R I_o T_o}$$

where Δt is the threshold pulse length to raise the reactants to the reaction temperature (T_R). T_R is taken to be 973°K. This value was estimated for temperature ranges found in the literature[2,6] for Si_3N_4 synthesis from SiH_4 and NH_3.

The calculated threshold pulse lengths in SiH_4 for initial laser intensities equal to 8 and 16 watts/cm^2 are shown in Fig. 9 as lines "a" and "b". The absorptivity as a function of pressure was taken as the P(20) value shown on Fig. 5. The calculated Δt values have approximately the correct value and correct pressure dependence for pressures greater than 0.075 atm. Below a pressure of 0.05 atm, it is apparent that this simplified model does not approximate the observed behavior; threshold pulse lengths increase sharply with decreasing pressure rather than continuing to decrease.

A constant mass flow was used in all these experiments and thus the gas velocity varied inversely with cell pressure. Even at the lowest pressure, the time required for a volume element to transit the full length of the heated gas column exceeds the longest investigated pulse length by a factor of 20. Since this ratio was generally substantially larger than 20, all of the experiments fulfilled pseudo-static conditions from the criteria of pulse length and residence time. The heat flux due to the gas flow rate at the reaction temperature is also negligible with respect to the laser beam power. Only 0.8 watts is required to produce an exit temperature of 700°C at a volumetric flow rate of 25 cm^3/min. Therefore, the rapidly increasing threshold pulse lengths with decreasing pressure do not result from either of these two dynamic effects.

The second solution to the heat flux equation treats the steady state case where absorbed heat is lost to the cold cell walls by conduction. For this case, the heat transfer rate per unit length ($\dot{Q}/L$) between the inner cylindrical column of heated gas and the cell wall is

$$\dot{Q}/L = 2\pi k \frac{T_i - T_o}{\ln(r_o/r_i)}$$

where k is the thermal conductivity of the medium, T_i and r_i are the inner gas column temperature and radius, T_o and r_o are the outer wall temperature and radius.

The heat generated per unit length of the absorbing gas column is

$$\dot{Q}/\Delta x = I_o \pi r_i^2 \alpha p \exp(-\alpha p x)$$

where the terms are the same as defined previously. Equating these two expressions and solving for pressure (p) with x = 0, gives the critical pressure where conduction heat losses with a gas temperature T_i just equal absorbed power in the first exposed volume element. For T_i equal to the reaction temperature (T_R), this procedure indicates the critical minimum pressure at which a reaction can be induced,

$$P_{crit} = \frac{2k}{\alpha I_o r_i^2} \frac{(T_R - T_o)}{\ln(r_o/r_i)} \quad .$$

With k (SiH_4) = 0.65×10^{-3} watts/cm°C, the critical pressures are 0.09 and 0.05 atm for I_o equal to 8 and 16 watts/cm^2, respectively and are indicated as lines "c" and "d" in Fig. 9. These critical pressures, at which the threshold pulse lengths should go to infinity, are in sufficient agreement with the behavior exhibited by the threshold experiments to conclude that conductive losses to the cold walls caused the departure from the assumed domination by sensible heat as was used in the first solution. The time required to establish fully developed steady state conduction in 0.1 atm SiH_4 is estimated to be approximately $40 - 50 \times 10^{-3}$ sec, by the equation

$$t = \frac{x^2}{4\kappa}$$

where κ is the thermal diffusivity.

Even though highly simplified, these solutions to the heat balance equation give an adequate description of the conditions required to initiate the chemical reaction.

A second set of solutions considers the propagation of a reaction through a partially absorbing reactant gas. Generally, the conditions for initiating and propagating a reaction are the same as were assumed in the threshold analyses. In addition, it was assumed that the gas becomes completely transparent to the laser light once the reaction occurs and also that the reaction exotherm does not affect the reaction. Computer calculations give the power absorbed in each volume element along the beam axis as a function of time and calculates the instantaneous local temperature in the same manner used for the threshold estimates in the first volume element. Reaction is assumed to occur when the local temperature reaches the reaction temperature (T_R). The extent of the reaction is followed by calculating the location of T_R for various time increments.

Representative results of these calculations are shown in Fig. 18. The curves marked 1-5 correspond to the times indicated in the caption. Curve "1" corresponds to the condition where the threshold has just been exceeded in the first volume element. Curves "2-5" track the propagation of the reaction (at the intersection of T(x) with the 973°K isotherm) through the partially absorbing reactant gas column. The velocity with which the reaction propagates through the reactants is derived directly from the penetration of the reaction as a function of time. Figure 18 was calculated for the SiH_4 partial pressure and the total pressure, both equal to 0.2 atm. Figure 19 summarizes the results of similar calculations for pressures ranging from 0.04 to 0.2 atm. The time intercept (at distance = 0) is the theshold time required to induce the initial reaction. A plot of these intercept times as a function of pressure will give the equivalent of curve "a" in Fig. 9, except in this case a constant αp product was assumed rather than using experimentally measured values for $\alpha(p)$. The reciprocal of the slopes of the time-distance curves are equal to the penetration velocities (V_p). The calculated values of V_p are indicated for each pressure. Similar calculations have been made for a wide range of laser intensities, gas mixtures and ambient pressures.

Results of the type derived from these analyses are extremely important for designing process experiments. In the orthogonal synthesis configuration, the gas must reside in the laser beam long enough for the reaction

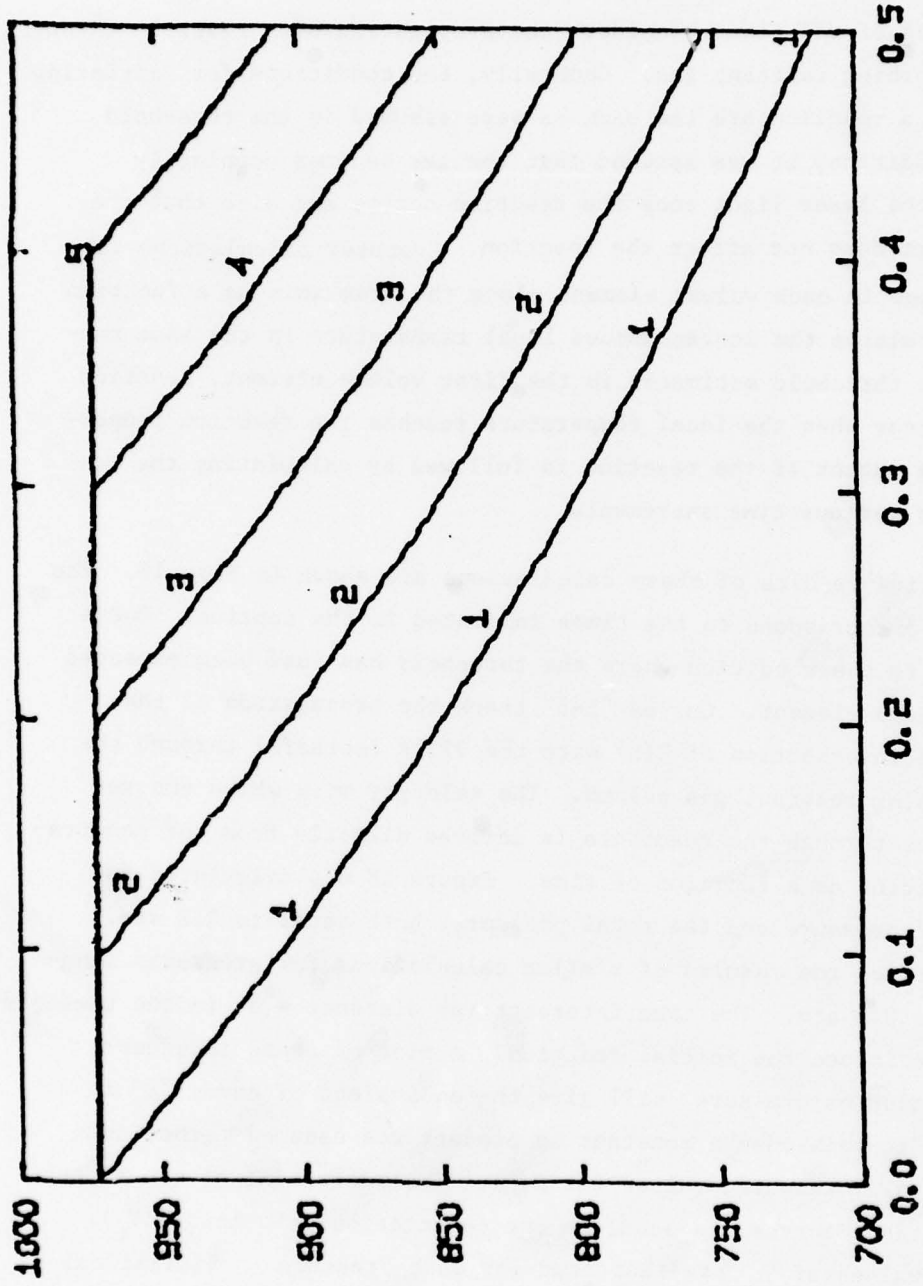

Figure 18. The temperature profile within 0.2 atm SiH_4 at various times after exposure to the laser beam. The times are: (1) 41 msec, (2) 43.2 msec, (3) 45.7 msec, (4) 48.1 msec, (5) 50.6 msec, after the laser beam is switched on. The beam intensity is 8 w/cm^2 and the product αp is assumed to be constant and equal to 0.6 cm^{-1}.

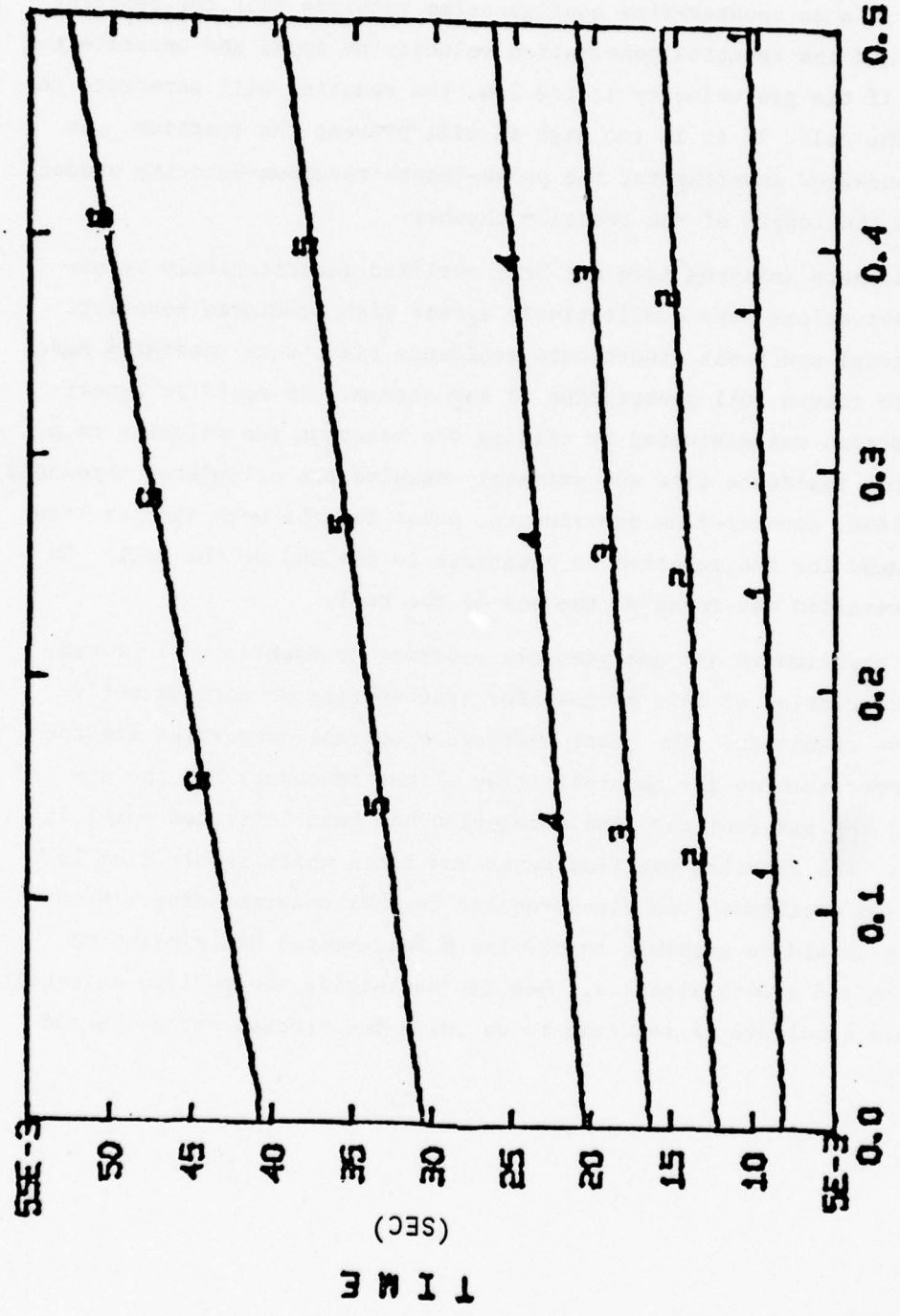

Figure 19. The time necessary to propagate the reaction zone to a specific distance for several SiH_4 pressures. The pressures are: (1) 0.04 atm, (2) 0.06 atm, (3) 0.08 atm, (4) 0.10 atm, (5) 0.15 atm, (6) 0.20 atm. The calculated propagation velocities are (1) 233 cm/sec, (2) 135 cm/sec, (3) 104 cm/sec, (4) 86.2 cm/sec, (5) 56.8 cm/sec, (6) 42.5 cm/sec.

to penetrate through the entire gas stream. With a thin reactant gas stream in this experimental configuration, the residence time needs to be only slightly greater than the threshold time, since the entire stream is subjected to an approximately uniform laser intensity. Achieving a stable position for the reaction in a cw counter-flow configuration requires that the reactant gas velocity and the reaction penetration velocity be equal and opposite to each other. If the gas velocity is too low, the reaction will penetrate to the back of the cell; if it is too high it will prevent the reaction. In pulsed, counter-flow experiments, the pulse-length·reaction-velocity product cannot exceed the length of the reaction chamber.

Although these analyses have not been verified quantitatively by experiment, observations have qualitatively agreed with predicted behavior. In the orthogonal synthesis experiments residence times were generally made long enough to insure full penetration of gas stream. In specific experiments the reaction was disrupted by raising the reactant gas velocity to a level where the residence time approximately equaled the calculated threshold time. In pulsed, counter-flow experiments, pulse lengths were shorter than times calculated for the reaction to penetrate to the end of the cell. No evidence of reaction was found at the end of the cell.

Further experiments and analyses are underway to develop an improved analytical description of this process for synthesizing powders directly from gas phase reactants. The least understood optical properties are the affect of temperature on the absorptivities of the reactants and the absorptivity of the gas from the time a reaction has been initiated until it is completed. The detailed gas flow paths and rates which result from laser heating and exothermic reactions require further understanding. With this base, is should be possible to develop a fundamental description of the nucleation and growth kinetics. Besides satisfying the obvious scientific interest, this knowledge is required to optimize the process variables and cell geometry.

III. Powder Size and Shape Modification

The feasibility of selectively interacting with oversize or high aspect ratio particles by means of high intensity light from a CO_2 laser source was investigated in this phase of the program. Selective heating causes particle size reduction by vaporization until decoupling occurs when the oversize particles reach a specific dimension. This approach is based on the diameter dependence of the absorption efficiency (Q_{abs}) which small particles exhibit to electromagnetic radiation. The Mie theory[14] shows that absorption efficiency decreases with particle diameter for particles which are small relative to the wavelength of the light. Once the particles begin to decouple and cool down, the vaporization rate will effectively stop because it is exponentially dependent on temperature.

The analytical basis for this approach and both the experimental procedures and results used to investigate its feasibility are presented in the following sections.

A. Theoretical

1. Power Absorbed by Particles

The power (P) absorbed in a particle subjected to an incident beam having a power density I (watts/cm^2) is:

$$P = IA_{proj}Q_{abs}$$

where A_{proj} is the projected area of the particle normal to the incident beam and Q_{abs} is the absorption efficiency.

The absorption efficiency (Q_{abs}) for spherical particles having a diameter (d) much smaller than the wavelength of the incident light (λ) is approximated by:[14]

$$Q_{abs} = -4X\,\mathrm{Im}\left\{\frac{m^2 - 1}{m^2 + 1}\right\}$$

where $X = \frac{\pi d}{\lambda}$ and $\mathrm{Im}\left\{\frac{m^2 - 1}{m^2 + 1}\right\}$ is the value of the imaginary part of the quotient derived from the complex index (m)

$$m = n - in'$$

where n and n' are the real and imaginary indices respectively. Both indices are wavelength and temperature dependent. The imaginary index (n') is related

to the absorption coefficient (α) by:

$$\alpha = \frac{4\pi n'}{\lambda} \quad .$$

For particles which are much larger than the wavelength, the absorption efficiency approaches

$$Q_{abs} = (1 - R)(1 - e^{-\alpha d})$$

where the reflectivity (R) is given by

$$R = \left(\frac{n - 1}{n + 1}\right)^2$$

2. Absorption Efficiency of Si_3N_4 Particles

The absorption efficiencies for the small and large particle cases can be estimated from an appropriate combination of the real and imaginary indices and the absorption coefficient. The high temperature values of the real indices at 10.6 μm can be represented by room temperature values with reasonable accuracy. For Si_3N_4, $n = 2.1$[15] at 10.6 μm. The values of the imaginary indices are less certain. The absorption coefficient of Si_3N_4 was calculated to be $\alpha_{10.6} = 8.24 \times 10^4 cm^{-1}$ at room temperature from transmission measurements through 0.5 μm thick films on Si substrates. The value of $n' = 6.95$, calculated from this α is probably a lower limit for a higher temperature approximation, since the fundamental absorption peak from the Si-N vibrational mode becomes more intense and broader with increasing temperature. This value of n' was used for calculation of Q_{abs}. These results are summarized in Table IV, and plotted in Fig. 20.

Figure 20 illustrates the fundamental characteristic which is being used in this approach to modify the size and shape of powders. Above a specific diameter, the particles absorb heat with a high efficiency that is independent of diameter. Below a specific diameter, the absorption efficiency decreases with diameter so the particles effectively decouple from the radiation. Diameter reduction via vaporization effectively stops once the particles begin to decouple, because the vaporization rate is exponentially dependent on temperature. This feature permits selective interaction with oversize particles. If they are heated long enough to cause dissociation, they can

TABLE IV. Optical Constants of Si_3N_4 for 10.6 μm Light

At $\lambda = 10.6$ m

$n = 2.10$

$\alpha = 8.25 \times 10^4$ cm^{-1}

$n' = \alpha\lambda/4\pi = 6.95$

$m_{Si_3N_4} = 2.10 - 6.95\ i$

For small d

$Q_{abs} = 0.0397d$ (d in μm)

For large d

$Q_{abs} = 0.874$

be eliminated from the powder avoiding subsequent problems with discontinuous grain growth and strength limiting flaws associated with oversize grains.

3. Heat Balance and Decomposition Rate

a. General

The power balance between the rate heat is absorbed by particles and the various heat loss mechanisms is given by

$$I \frac{\pi d^2}{4} Q_{abs} = C_p \frac{\pi d^3}{6} \rho \frac{dT}{dt} + h\pi d^2 (T - T_{amb}) + \varepsilon\sigma\pi d^2 (T^4 - T_{amb}^4) + J\pi d^2 \Delta H$$

where I = beam intensity

d = particle diameter

Q_{abs} = Mie absorption efficiency

C_p = specific heat

ρ = density

T = absolute temperature

t = time

h = convective heat transfer coefficient

ε = emissivity

σ = Boltzman radiation constant

J = specific molar vaporization rate

ΔH = molar heat of vaporization.

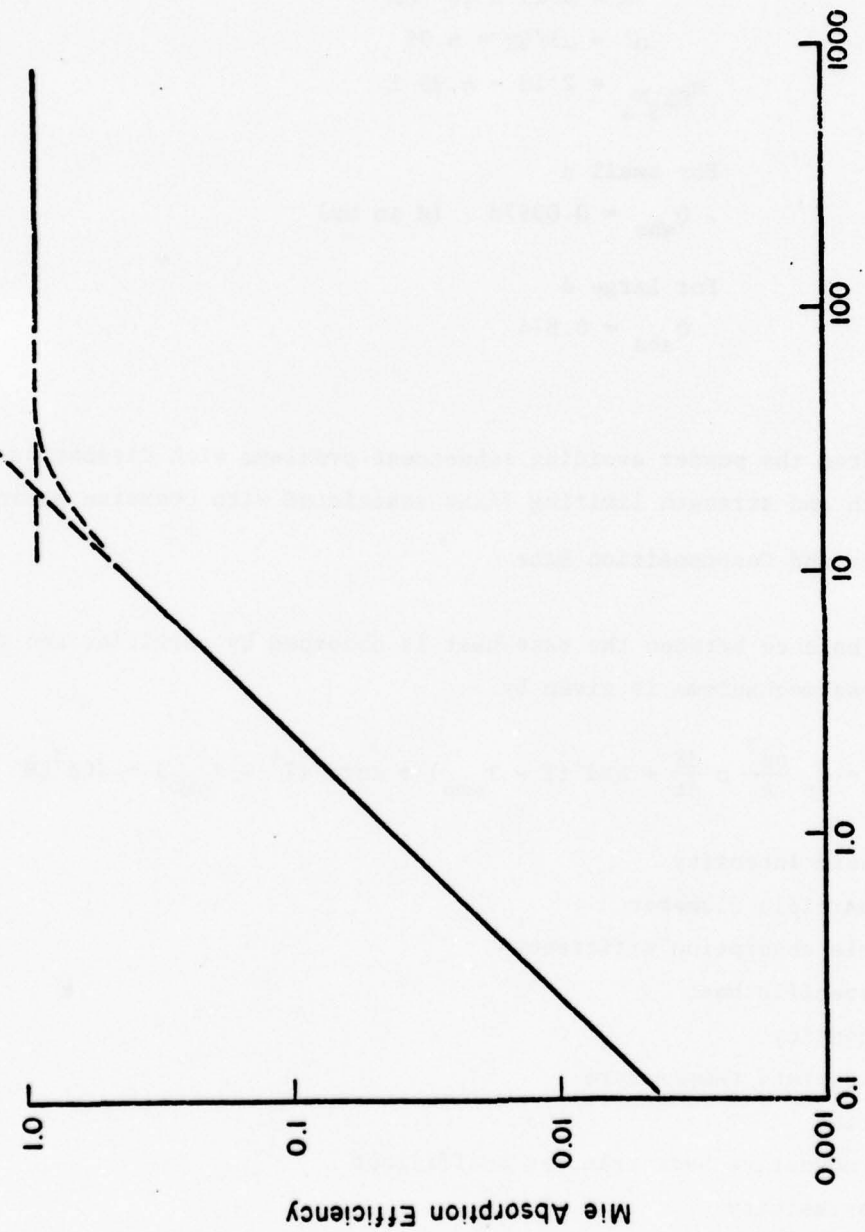

Figure 20. Mie absorption efficiency of Si_3N_4 particles to 10.6 μm light as a function of particle size. See text for assumptions and material properties used in these calculations.

At least one parameter in each of the terms making up this equality requires judicious assumptions since the conditions to which the particles are submitted are so unusually extreme. The procedures used to evaluate the absorption efficiency (Q_{abs}) have already been presented and the power intensity in an off-focus light beam (I) will be discussed later. The most critical assumptions lie in the identification of the vaporization model and, therefore, the dependence of vaporization rate (J) on temperature and ambient conditions as well as the estimation of the heat of vaporization (ΔH). It is also apparent that particle size reduction can occur by a variety of fracture and spalling mechanisms rather than vaporization.

Like other analyses appearing in the literature,[16,17] our analytical description of the vaporization process is based on the Knudsen-Langmuir equation:[18]

$$J = (P_e - P)(2\pi MRT)^{-1/2}$$

where $(P_e - P)$ is the difference between the equilibrium vapor pressure of the volatile species (Pe) and its pressure in the ambient (P) and the molecular weight of the species is M. This model explicitly assumes that the density of the vapor cloud is sufficiently low that no significant diffusional resistance is offered to the emitted molecules. This is probably not a valid assumption for extremely high vaporization rates which these particles experience at relatively high ambient pressures, but an analysis in terms of this model is useful because it provides an estimate of the absolutely maximum vaporization rate which might be expected if the necessary mass transport and power input criteria can be satisfied. We will show later that the power balance is virtually completely dominated by the $J\Delta H$ term once an endothermic reaction begins. Ignoring the small effect of transient time, one can determine the extent of a decomposition or sublimation reaction from the power absorbed without specifying the exact mass transfer process(es) by which it proceeds.

b. Beam Intensity (I)

The intensity of the laser beam may be adjusted by operating at various locations relative to a focusing element (lens or mirror). For locations which are not close to the focal point, a linear convergence from the initial beam diameter to a point is a good approximation of the nominal beam

size. The power distribution within the beam is nominally gaussian, but it must be mapped if this information is required for locations not close to the focal point.

Near the focal point, the gaussian power distribution approximation is valid but the beam size does not converge linearly to a point. The exact description depends on a number of factors including the energy and wavelength distributions in the emitted light beam. Dickson[19] has analyzed the $1/e^2$ radius of a propagating gaussian beam as a function of initial radius and lens focal length. The results of these calculations applied to the CO_2 laser and 5 inch nominal focal length lens used in these experiments are given in Figs. 21 and 22. Figure 21 shows experimentally measured "burn spot" radii as well as the calculated beam radius as a function of distance from the lens. Figure 22 is an expansion of the region near the focal length. The power densities are calculated on the basis of a 170 watt maximum emitted cw power. The peak power in the pulsed mode is approximately 5-10 times higher than the maximum cw power level. The maximum power density which we can achieve with the available equipment in its present configuration is approximately 2×10^5 watts/cm^2 in a cw mode and in excess of 10^6 watts/cm^2 in a pulsed mode. Modifying the equipment to use a 2½ inch focal length lens will reduce the minimum beam radius by approximately a factor of two, giving power densities which are four times higher; however, injecting the particles into the center of a 180 μm diameter region presents a difficult problem.

C. Particle Heating Rate and Comminution Time

The expression equating the power absorbed by a particle to the heat dissipation mechanism has been solved for various Si_3N_4 particle diameters, beam power densities and ambient conditions.

Two decomposition mechanisms have been considered. In the first, which is typical of normal vaporization kinetics, Si_3N_4 decomposes to Si (liquid) and N_2 (gas). The heat of this decomposition reaction is 8.6×10^5 joules/mole.[20] The vapor pressure (Pe) used in the Knudsen-Langmuir equation was the equilibrium vapor pressure of Si_3N_4. We have also postulated that at higher vaporization rates, stoichiometric vaporization to Si(gas) and N_2(gas) will occur. The heat of sublimation is calculated to be 2.0×10^6 joules/moles.[20] In this case the rate controlling step was assumed

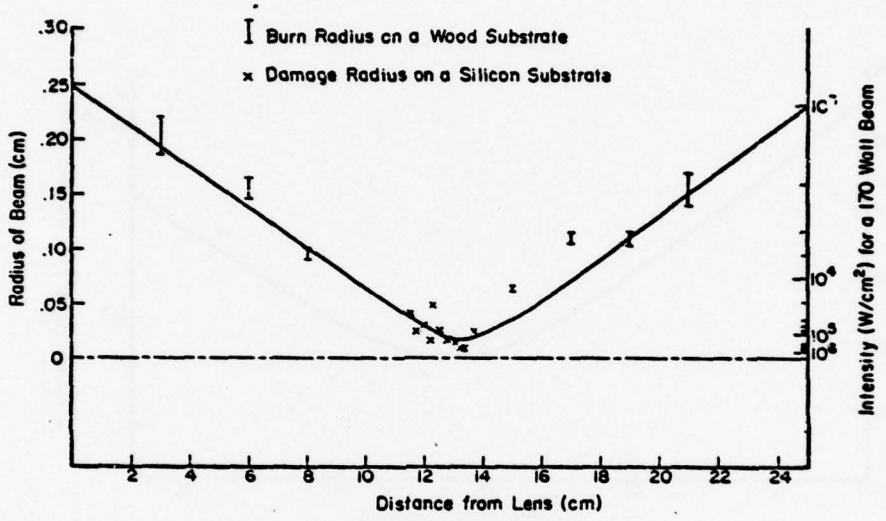

Figure 21. Beam radius to $1/e^2$ intensity points as a function of distance from a 13 cm focal length lens. A gaussian energy distribution is assumed.

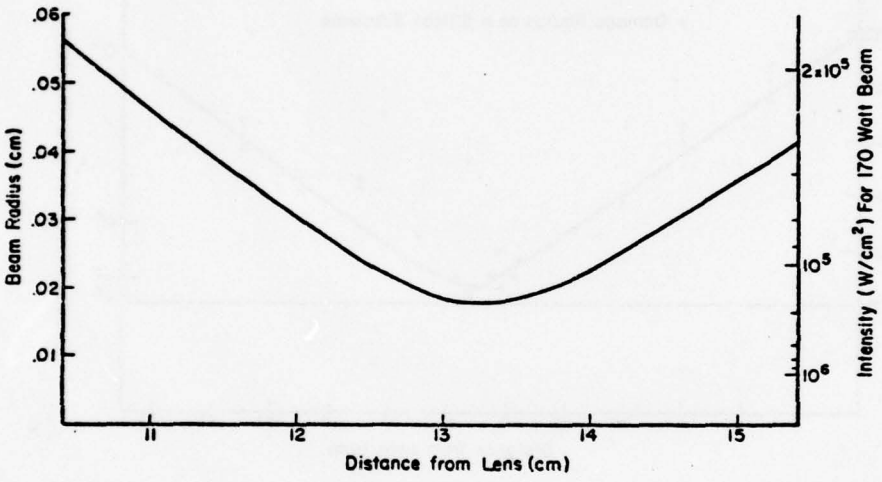

Figure 22. Beam radius to $1/e^2$ intensity points for region near the focal point. A gaussian energy distribution is assumed.

to be the volitilization of silicon. Therefore, Pe was equal to the vapor pressure of silicon (liquid or solid).[20] The first reaction will leave a Si particle if the reaction proceeds to completion, which has a diameter equal to 94% of the diameter of the original 100% dense Si_3N_4 particle. Partial decomposition will produce a Si skin on a Si_3N_4 core. The sublimation reaction will leave a reduced diameter Si_3N_4 particle.

The results of these calculations are summarized in Fig. 23 and in Table V. The h = 0 results are for particles heated in vacuum and h = 0.077 ($w/cm^2 °K$) is representative of a heat loss coefficient with a turbulent boundary layer in 1 atmosphere pressure air.

TABLE V. Calculated Residence Times for Heating, Decomposing and Causing Diameter Reduction by Sublimation

- Decomposition

  $Si_3N_4(s) \rightarrow 3Si(\ell) + 2N_2(g)$

  $\Delta H = 8.6 \times 10^5$ Joules/mole[20]

- Sublimation

  $Si_3N_4(s) \rightarrow 3Si(g) + 2N_2(g)$

  $\Delta H = 2.0 \times 10^6$ Joules/mole[20]

	Decomposition			Sublimation (30 → 20 μm)		
I w/cm^2	T_∞(°K)	$t(T_\infty)$(sec)	Δt(sec)	T_∞(°K)	$t(T_\infty)$(sec)	Δt(sec)
10^3(h = 0)	1670	15.0×10^{-3}	20.8×10^{-3}	2190	25.0×10^{-3}	135.0×10^{-3}
10^4	1815	1.4×10^{-3}	7.26×10^{-3}	2530	1.9×10^{-3}	12.9×10^{-3}
10^5	1950	0.15×10^{-3}	0.73×10^{-3}	2915	0.25×10^{-3}	1.35×10^{-3}

T_∞, reaction temperature plateau; $t(T_\infty)$, time to reach reaction temperature; Δt, residence time to complete reaction at T_∞

The time-temperature history experienced by a particle is accurately approximated by a linear temperature rise to the decomposition temperature followed by an approximately constant temperature plateau (T_∞) which persists until the absorption efficiency (Q_{abs}) decreases because the particles become

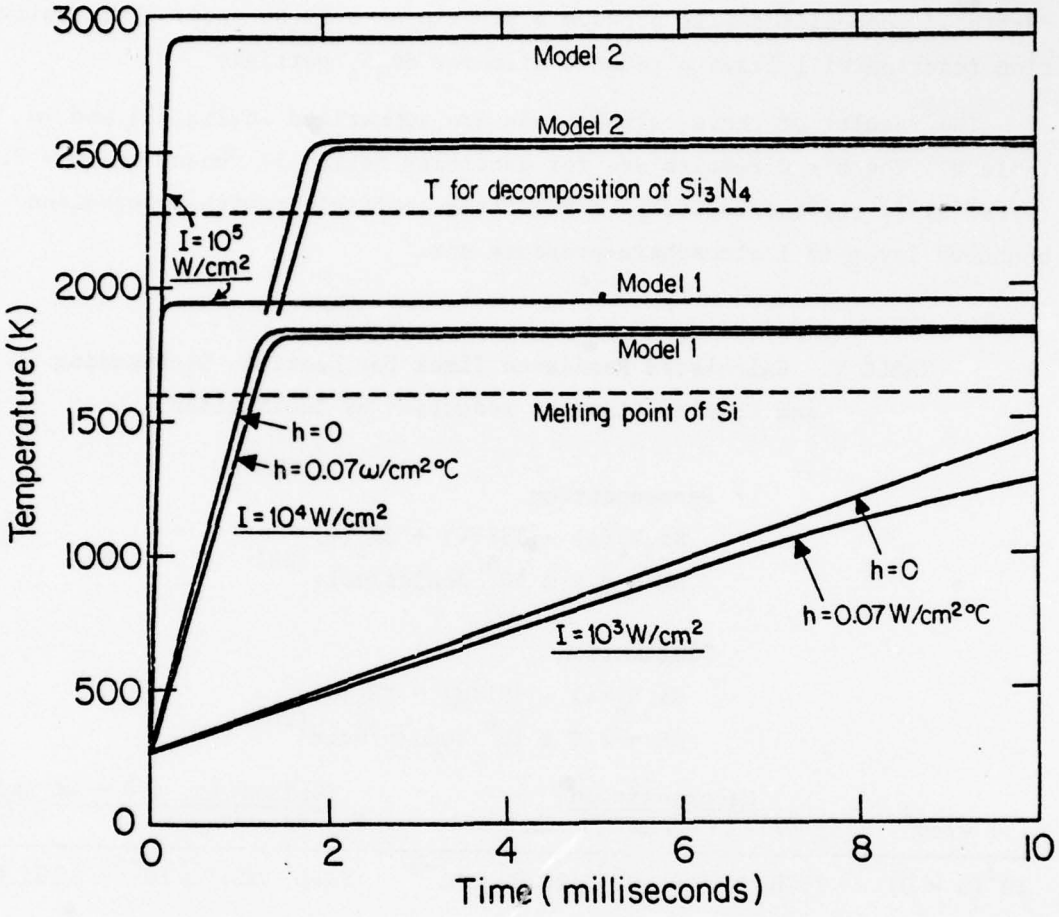

Figure 23. Temperature versus time for 30 μm Si_3N_4 particles irradiated at three different intensities. The heat transfer coefficient of h = 0 corresponds to a vacuum and h = 0.077 w/cm^2 is a high value corresponding to a turbulent boundary layer. Large particle behavior is assumed; therefore, Q_{abs} is taken as constant with time and temperature (Q_{abs} = 0.875).

too small to couple efficiently. The initial heating rate is dominated by sensible heat for power densities (I) greater than 10^3 watt/cm^2. For $I \leq 10^3$ watt/cm^2, conductive heat losses have some effect. In the plateau region, the absorbed power is dominated by the $J\Delta H$ term of the endothermic reaction. The actual temperature levels (T_∞) of the plateaus result from the assumptions inherent in the Knudsen-Langmuir model and are probably subject to some error. These errors will not seriously affect the time estimate to reach the decomposition temperature ($t(T_\infty)$) because the decomposition reaction must occur within a temperature range of approximately 10^3°K and the heating rates are of the order of 10^6°K/sec. Also, the transient time to reach the decomposition temperature is typically almost an order of magnitude smaller than the residence time required for the endothermic reaction at T_∞. Therefore, the estimate of the exposure time (Δt) required to induce comminution is insensitive to the potential errors resulting from the Knudsen-Langmuir model.

We recognize that these two model responses of the particles to the laser are both simplified and idealized. The particles may respond in a number of possible ways which involve different diameter reduction mechanism and rate controlling processes. For instance, nonisotropic vaporization can self-propel the particles out of the assumed trajectory at nearly sonic velocities. The vaporization products may shield the particles from the incident radiation and either absorbed water, shockwaves or rapidly expanding N_2 gas could cause the particles to explosively eject debris by non-vaporization processes.

B. Experimental

Two types of experiments have been used to investigate the use of high intensity light for modifying the size and shape of refractory particles. In static experiments, particles are supported by a transparent substrate and subjected to light pulses of varying intensity and duration. In flight experiments, powders are entrained in a gas stream and passed through varying intensity cw beams at varying velocities.

In the static experiments both the exposure times and the exact region where particles interact with the light can be precisely controlled. With the laser employed in this program, the maximum power densities in the pulsed mode were 5-10 times higher than could be achieved in cw mode. Also, it is straightforward to isolate those particles which have interacted with the laser for

purposes of diagnostic characterization. These are important features for establishing controlled experiments over an extended range of process variables although the substrate clearly introduces uncertainty about reflected light and interactions between the heated particles and the hopefully cold substrate.

Over moderate ranges of ambient pressure and particle velocities, the flight experiments are controllable; however, at minimum particle velocities and minimum ambient pressures, control over the exposure times and particle trajectories becomes less certain. Even though the flight experiments are less precise in terms of our ability to define and control experimental conditions, they are much cleaner than the static experiments. Also, they simulate a configuration which would be used in a production process.

1. Static Experiments

In the static experiments, powders were spread on polished Si wafers and subjected to varying duration and intensity light pulses. After being subjected to the pulse, they were examined microscopically to determine the conditions which caused particle size reduction. Conditions were catagorized into three groups depending on whether they exhibited (1) no particle size reduction, (2) diameter reduction less than 50% of initial diameter and (3) diameter reduction greater than 50% of initial diameter. Pulse lengths varied from 10^{-3} to 1 second; power density varied between 10^{4} to 10^{6} watts/cm^{2}.

Clean Si wafers were subjected to pulses over the entire I-t range used to study particle size reduction without causing any visible cratering or melting. Under the most severe conditions, an interaction between the substrate and the particles was evident. This had the character of melting and engulfing the particles or of cratering. No damage or interaction was evident under pulse conditions which just caused particle size reduction. Thus, the threshold values were not affected by the interaction. The results of these static experiments are shown in Fig. 24.

2. Flight Experiments

The "flight" particle size reduction experiments were carried out in the apparatus shown in Fig. 8.

Particles were entrained in a variable velocity gas stream and injected into the laser beam by means of the powder injector tube. After passing

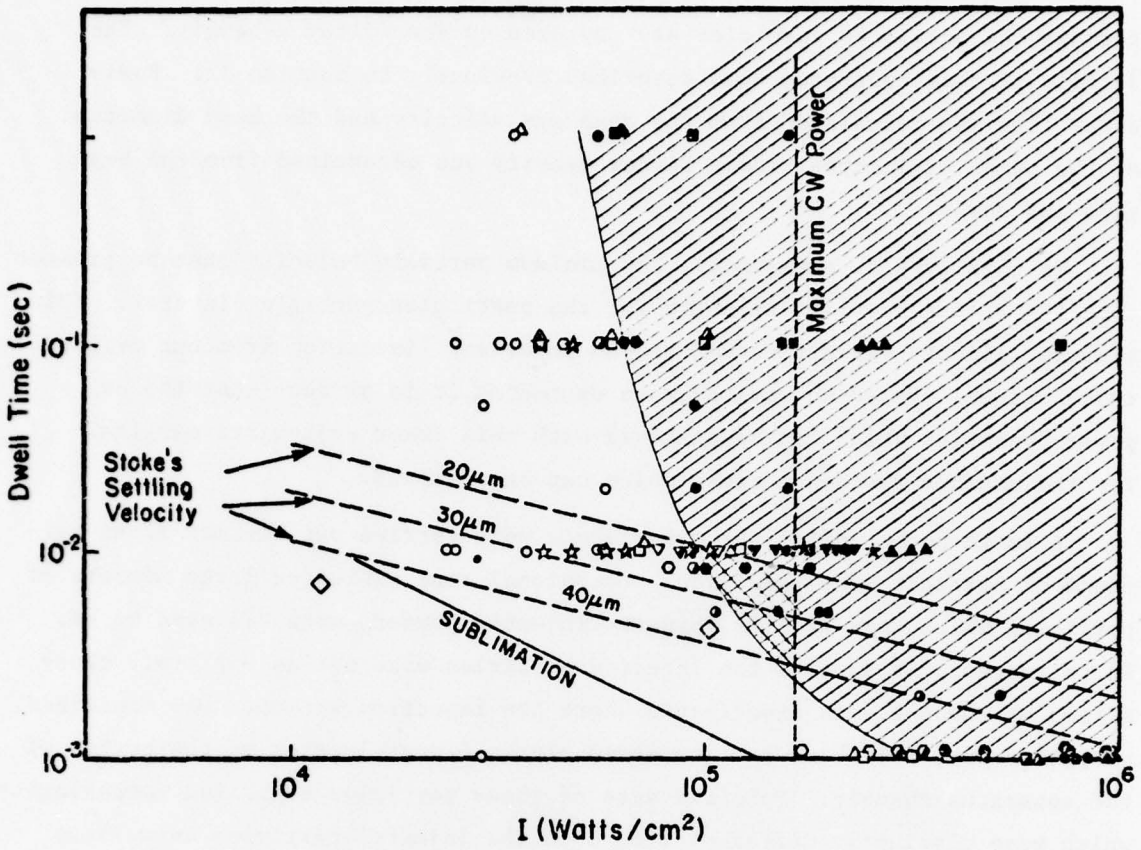

Figure 24. Summary of exposure times and laser intensities investigated for laser comminution of Si_3N_4 particles. See text for explanation of cross-hatched regions and demarcation lines.

Key: Diameter Reduction: ●, ■, ▲, etc. size reduction > 50%
◐, ◪, ◭, etc. size reduction < 50%
○, □, △, etc. no size reduction

Process Conditions:

- ○ , static expt., 1 atm Ar, d_o = 30-38 μm, reaction bonded Si_3N_4
- □ , static expt., 1 atm Ar, d_o = 20-30 μm, reaction bonded Si_3N_4
- △ , static expt., 2 Torr air, d_o = 20-30 μm, reaction bonded Si_3N_4
- ▽ , static expt., 1 atm air, d_o = 20-30 μm, reaction bonded Si_3N_4
- ⬡ , static expt., 1 atm Ar, d_o = 20-30 μm, hot pressed Si_3N_4
- ☆ , static expt., 1 atm Ar, d_o = $\leq$ 20 μm, hot pressed Si_3N_4
- ◇ , flight expt., 1 atm air, d_o = 20-30 μm, reaction bonded Si_3N_4

through the beam, the particles are captured on the filter assembly. The details of this apparatus were described previously in Section II. Residence time was calculated from the mean gas velocity and the beam diameter at the point of intersection. Powder density was determined from the beam size and power.

In this type of experiment, the minimum particle velocity must be greater than the Stokes settling velocity for the particular particle diameter. This minimum velocity was not considered an important limitation from our original calculations. Based on revised rate estimates, it is evident that the cw power densities which can be achieved with this laser system are marginal for the maximum residence times which can be achieved.

A large number of flight experiments were carried out without clear evidence of particle size reduction. Occasional runs exhibited large numbers of particles which were smaller than the injected powders were believed to be. In retrospect, it appears the injected particles were not as uniformly classified as thought. In experiments where the injection velocity was minimized, particles were collected on tape or in aluminum pans located on the bottom of the apparatus chamber. Specific sets of these particles exhibited morphologies which were distinctly different from both the injected particles as well as the particles whose diameters where reduced in the static experiments.

Two types of particle trajectories were observed in these flight experiments. Predominately, an incandescent plume of hot particles originated at the point where the injector tube axis and the beam axis intersected. At high gas velocities this plume extended with some radial expansion along the direction of the injection tube. At lower velocities the plume slumped downward under the influence of gravity. As one would expect, the plume appeared hotter at lower velocities. Although the measurement is subject to several sources or error, microoptical pyrometer measurements indicated particle temperatures in the range 1750-1900°C. Qualitatively, this is the range expected from the heating rate calculations. In the second trajectory, particles originating from the same point followed a downward pointing cone along the direction of the beam. These particles were evidently self-propelled by non-isotropic vaporization.

Typical conditions for flight and static experiments are shown in Fig. 24.

3. Results and Analyses

The results of these experiments have answered fundamental questions and have provided operational gudielines for a process which has not been studied previously. Some of these issues are:

- Determination whether light induced comminution is feasible
- Development of empirical intensity-time-ambient conditions which result in particle size reduction
- Correlation with alternative rate contolling processes leading to an understanding of the kinetics and the mechanism
- Decoupling at specific particle sizes to achieve selective interaction with oversize particles.

Figure 24 summarizes experimental conditions which have been investigated, indicates operational limits which are accessible with the existing equipment and shows the predicted times required for diameter reduction by the sublimation model.

The triangles, circles, and squares indicate the conditions employed with the static, pulsed experiments. The single cross-hatched region at the right of the figure indicates the conditions which resulted in diameter reduction. The line which bounds the cross-hatched region indicates the combinations of pulse length and power density which caused approximately a 50% diameter reduction. There was no evidence of the Si substrate interacting with the particles for conditions near those represented by this line. These static, pulsed experiments demonstrate that controlled comminution can be caused by specific exposures to high intensity light. They also show why it is virtually impossible to cause comminution in flight experiments within the operational limits imposed by existing equipment.

The maximum power density which can be achieved in the cw mode is shown by the verticle, dashed line at approximately 2×10^5 watts/cm^2. This corresponds to the maximum emitted power (about 170 watts) focused to the diffraction limited spot size through a 5 inch focal length lens (about 0.04 cm). The three diagonal, dashed lines, marked 20, 30 and 40 μm, indicate the times required for particles of these diameters, travelling at their Stokes setting velocities, to pass through beams focused to diameters which correspond to the indicated power density with the laser emitting 170 watts. The envelope of I-t conditions which are accessible with the existing equipment is confined to the region below the dashed line corresponding to each specific particle

size, because it is not possible to entrain and transport particles at velocities slower than their Stokes settling velocity in most experimental configurations. Based on the results of the static, pulsed experiments, the only set of I-t conditions where comminution can be anticipated in flight experiments is shown by the double cross-hatched, triangular region at power densities ranging from approximately 1-2 x 10^5 watts/cm^2 and dwell times from 2-10 x 10^{-3} seconds.

Experiments were conducted at I-t conditions corresponding to this region; however, it proved difficult to capture powders which had been subjected to a defined history with any sense of certainty. The photomicrographs presented later show particles which were comminuted by flight experiments. While limitations imposed by existing equipment prevented a thorough examination of comminution with flight experiments, it is apparent that these experiments are possible with commercially available CO_2 lasers. Based on the static experiments, the process should operate within readily controllable conditions using a 1500 watt laser.

The static experiments examined the effects of particle size, particle density, ambient atmosphere and ambient gas pressure. The specific values were:

Particle sizes: $\leq$ 20 μm, 20-30 μm and 30-38 μm

Particle density: 60 and 100% of theoretical

Ambient atmosphere: air and argon

Ambient gas pressure: 2 Torr and 1 atmosphere.

Within the precision of the observations, none of these variables caused any systematic variation in the I-t required to achieve approximately 50% diameter reduction. The line captioned "sublimation" represents the calculated times required to reduce the diameter of Si_3N_4 particles from 30 to 20 μm (the seventh column in Table V). These results also do not follow the I-t behavior predicted on the basis of a sublimation process which is rate controlled by the level of absorbed power.

The discrepancy between the assumed model and the observed behavior is not understood in detail. Most of the deviations which we can postulate would make the agreement better at lower power densities and worse at higher power densities in contrast to actual behavior. One possible explanation is that at

lower power densities, the Si_3N_4 particles partially decompose forming a Si skin which decouples them from the laser. At high temperatures, Si will reflect as a metal because free carriers are thermally excited. If this is the reason for the observed discrepancy, the overall vaporization process may still be rate controlled by absorbed power but the absorption efficiency (Q_{abs}) will be lower than expected. A reduced value of Q_{abs} would also shift the predicted sublimation behavior in a direction which is closer to the observed behavior. X-ray diffraction analyses which are discussed later support this model because comminuted particles contained both Si_3N_4 and Si phases. Generally these powders also exhibited a metallic luster.

The absence of a particle size dependence on the I-t conditions required to cause a 50% diameter reduction is consistent with the particles behaving as "small" particles as defined previously and shown in Fig. 24. Also, small particle behavior will result in Q_{abs} being lower than expected and thus may be responsible for the discrepancies discussed above.

With absorbed power rate limiting, the diameter reduction rate $\left(\frac{dd}{dt}\right)$ is given by

$$\frac{dd}{dt} = - \frac{MIQ_{abs}}{2\rho\Delta H}$$

where M = molecular weight

ρ = density of the particle

I = local beam intensity

ΔH = molar heat of vaporization

Q_{abs} = absorption efficiency.

For large particles, the absorption efficiency is independent of particle size. For small particles it is approximated as linearly dependent on particle size ($Q_{abs} \simeq Cd$) where the proportionality constant (C) is dependent on optical properties of the constituent materials. Thus, for small particles

$$\frac{dd}{dt} = - \frac{MICd}{2\rho\Delta H}$$

Where these expressions are integrated and normalized to the initial diameter (d_o) they give

Large particle behavior:

$$\frac{d}{d_o} = 1 - \frac{MIQ_{abs}(t - t_o)}{2\rho\Delta H d_o}$$

Small particle behavior:

$$\ln(d/d_o) = - \frac{MIC(t - t_o)}{2\rho\Delta H}$$

Thus, with small particle behavior, the $I_o(t - t_o)$ product required for a fixed d/d_o (e.g., 50%) is independent of particle size. For large particle behavior, the $I_o(t - t_o)$ product for a fixed d/d_o is linearly dependent on d_o.

The absence of either ambient pressure or atmosphere effects also follows if the vaporization process is rate controlled by absorbed power, because none of the possible kinetic effects (e.g., boundary layer, surface oxides, etc.) are rate controlling. When preliminary flight experiments did not exhibit comminution under conditions predicted by the Knudsen-Langmuir model, there was speculation that SiO_2 formed on the particles suppressing vaporization. These results indicate that the oxide is not a factor at these high vaporization rates.

The photomicrographs, Figs. 25, 26, and 27, show Si_3N_4 particles which have been subjected to the CO_2 laser beam. The central region of Fig. 25 is the area which was pulsed in a static experiment and it along with Fig. 26, illustrate that 20-30 μm diameter particles are reduced in diameter to 10-20 μm. The 8 μm diameter particle shown in Fig. 27 was caught on the filter after passing through the beam in a flight experiment. By the absence of a solidification morphology or texture, we conclude the Si_3N_4 core remained largely in tact and that there was very little liquid Si produced in these experiments. We also conclude by the approximate equality between the number of particles per unit area of substrate in the irradiated and non-irradiated regions, as well as the size of the comminuted particles in relation to the uneffected particles, that the comminution process does not result from splitting or fracturing the particles into pieces which are major fractions of the original particle, i.e., they don't fracture into halves, thirds, or quarters, etc. This result indicates that the diameter of these particles was reduced either by vaporization or by ejecting very small pieces of debris by an undefined mechanism.

Particles like those shown in Fig. 28 are produced in maximum power intensity flight experiments, but they were caught in a direction roughly parallel to the direction of the laser beam, rather than on the filter along the path of their injected trajectory. They were evidently self-propelled by

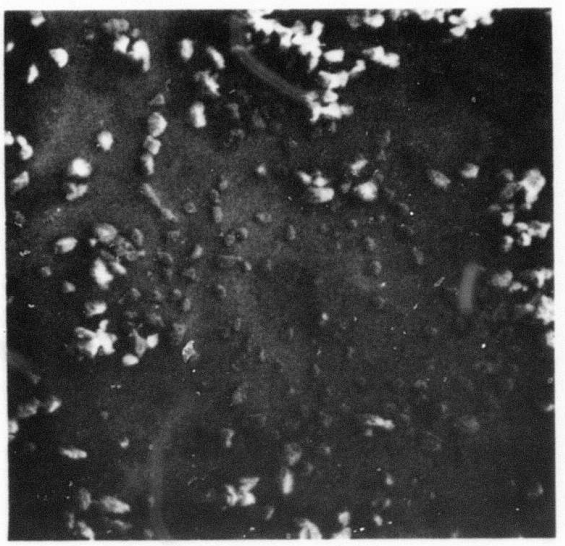

Figure 25. An example of Si_3N_4 particle size reduction caused in static, pulsed experiments. The central region shows the reduced particles. Pulse conditions were: 10 msec pulse, $I \simeq 2 \times 10^5$ w/cm^2. (100x)

Figure 26. Reduced diameter Si_3N_4 particles near center of region subjected to laser pulse. (1000x)

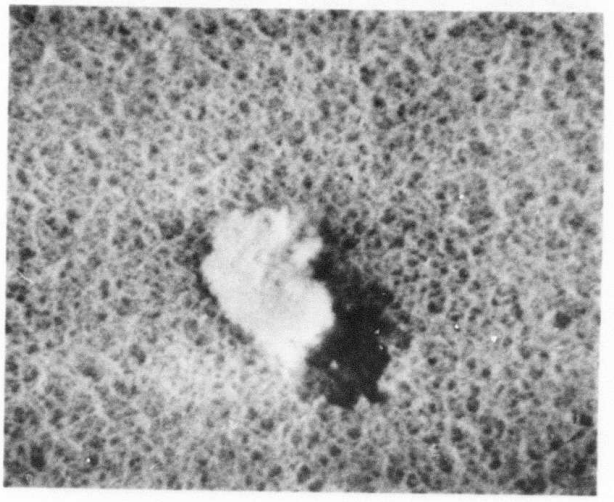

Figure 27. Reduced diameter Si_3N_4 particle captured on filter in cw, flight experiment. (3000x)

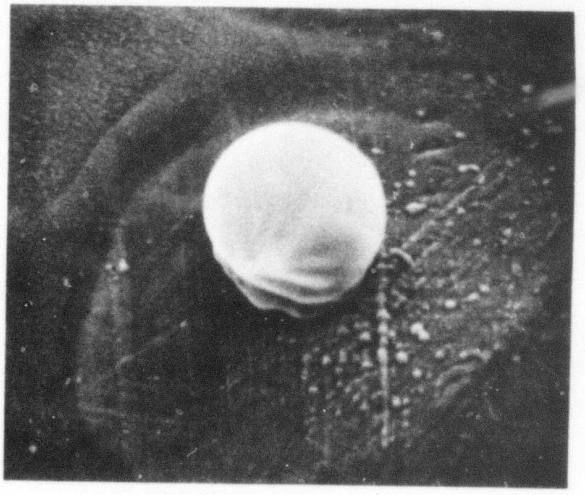

Figure 28. Reduced diameter, spherodized particle captured along laser beam axis in cw, flight experiment. (1000x)

nonisotropic vaporization. These particles were clearly liquid at some time based on their smooth spherical morphology, and have final diameters which are essentially equal to the original particles. Both characteristics are expected if the Si_3N_4 particles decompose to Si liquid and N_2 gas.

X-ray analyses have been used to characterize the powders, but quantities of comminuted particles have been so limited that it has not been possible to do an extensive a phase analysis as we would have liked. Powder particles whose diameters were reduced in the static experiments were analyzed by Debye-Scherrer diffraction. These powders contained both Si_3N_4 and Si phases. The volume fractions were not estimated by quantitative techniques but the peak heights are roughly equivalent indicating that there may be more Si present than is suggested by their morphologies. There were not enough spherical particles, as shown in Fig. 28, to use for diffraction analysis. These particles revealed only Si by x-ray probe analysis (EDAX) which showed that they had not been contaminated by the Al pans but gives no information regarding the N_2 content. It appears reasonable to assume that they are completely Si based on their morphology.

These results indicate that two distinct reaction mechanisms can result when Si_3N_4 particles are subjected to high intensity 10.6 μm radiation. It appears that they decompose or sublime according to either

$$Si_3N_4(s) \rightarrow 3Si(\ell) + 2N_2(g)$$

or

$$Si_3N_4(s) \rightarrow 3Si(g) + 2N_2(g)$$

depending on the power density and exposure time. Much careful work is required to confirm that these are the operating mechanisms and to identify the conditions where each dominates. Both mechanisms can be used to advantage if adequately controlled. Controlled sublimation should result in uniform size, spherically shaped particles as was initially proposed. Partial decomposition of Si_3N_4 particles should leave a Si skin on the Si_3N_4 cores which is the composite structure proposed for reactive sintering. We will also attempt to form particles with this structure by pyrolizing a gaesous Si reactant onto laser heated Si_3N_4 particles.

IV. Summary and Discussion

During the first year of work, we have investigated two laser heated processes for producing powders with characteristics which will make them superior for subsequent consolidation in finished parts. In the first, powders have been produced directly from laser heated gas phase reactants. In the second, the size and shape of over-sized or elongated particles have been selectively reduced to acceptable dimensions by a laser heated vaporization process. Because of its importance for high temperature engine components, our work has concentrated on silicon nitride ceramics. Both Si_3N_4 and Si powders have been processed. The latter powders are used for reactive sintering processes. These tasks have involved processing experiments, material characterization and analytical modeling. The two processes are sufficiently distinct that they are summarized separately.

• Powder Synthesis

Both Si and Si_3N_4 powders have been synthesized from SiH_4 or NH_3/SiH_4 mixture gas phase reactants. Heating was accomplished by direct absorption of the nominally 10.6 μm light by the reactants. Static and flowing-gas synthesis processes have both been investigated. Flowing-gas processes were developed in configurations where the reactant stream and the laser beam intersected orthogonally as well as in opposite, coaxial directions (counter-flow). The exposure times and beam intensities which were investigated ranged from those required for unimolecular, multiphoton reactions to those of more nearly conventional thermal reactions. A wide range of process variables have been systematically investigated and many of the process characteristics are understood to a first order.

Fundamentally, the most important result is that both SiH_4 and NH_3 couple effectively to highest gain emissions from a CO_2 laser. Consequently, it was feasible to induce the desired chemical reactions. Powders were formed with time-intensity conditions ranging from 10^{-9} seconds, 10^7 watt/cm^2 pulses to cw exposures at intensities as low as 8 watts/cm^2.

It appears that the powders which resulted from the short pulse, high intensity conditions did not form by unimolecular, multiphoton processes. Rather, it appears that a plasma was induced by the high electro-magnetic fields and that the reaction was brought about by the localized heating. Absorptivities are being measured at other emission lines to determine whether there are more favorable wavelengths to attempt unimolecular reactions.

The thermal reaction domain has been studied and analyzed. A first order model of the heating and subsequent reaction is one of a spontaneous reaction at a critical temperature. This model correlates well with observed time-intensity effects. At high intensities the process is controlled by sensible heat. At lower intensities, conductive heat losses become increasingly important.

Both Si and Si_3N_4 powders have been produced and characterized. Powders were characterized by x-ray diffraction, electron diffraction, TEM, STEM, IR spectroscopy, BET, and wet chemical techniques. Particle diameters range from a minimum of 25-35 Å to approximately 1000 Å. The smallest particles were produced at the shortest, highest intensity pulses and they got larger as the intensity was decreased. The Si_3N_4 particles had a narrower range of diameters than the Si particles. Gram sized quantities of Si_3N_4 powders were produced with directly observed particle diameters entirely within the range of 100-200 Å. The best Si powders generally ranged from 200-600 Å, with a few particles in the range of 600-1000 Å. Characterizations indicated that these equiaxed particles are either amorphous or are of extremely small grain size, highly distorted crystals. Preliminary results indicate that the latter may be the case. Characterization with direct lattice imaging and dark field electron microscopy techniques is continuing to clarify this point, because it is important for defining the driving forces which are operative during sintering. The particles have smooth surfaces and no open cell porosity.

The Si and Si_3N_4 powders produced during these nonoptimized processing experiments exhibit better diameter uniformity than has been achieved previously. Also, the process will be highly efficient energetically. The entire laser beam is absorbed within an optical path length of a few centimeters. Even if all of the thermal energy is provided by a CO_2 laser, the energy investment in powder synthesis will be approximately 2.5 kw hr/kg of Si_3N_4 (from $SiH_4/10NH_3$). It can be reduced further by using more efficient preheating methods or exchanging heat between entering and exiting gases. It appears probable that this synthesis technique will emerge as an important process.

• Particle Size and Shape Modification

The controlled modification of particle size and shape by subjecting them to high intensity illumination was successfully demonstrated. Process

models give reasonably good agreement between analytical and observed behavior.

Experimental results indicate that two vaporization processes probably occur. At the highest intensities, Si_3N_4 particles vaporize as Si(g) and N_2(g). At lower intensities, they apparently decompose by losing N_2(g), leaving molten Si.

The intensity-time exposures required to cause particle size reduction are substantially more severe than were predicted in our original analyses of the process. This discrepancy changed the process from being easily achievable with a 150 watt laser to being very marginal with that power level. Consequently, most of the mapping of conditions which cause comminution was done with supported particles in a pulsed laser mode. Longer, higher intensity exposures were realized than could be achieved with cw, gas entrained experiments.

These experiments demonstrated particle size reduction, leaving equiaxed particles. They did not demonstrate the decoupling which will cause the predicted termination of the comminution process at a specific particle size. These experiments could not be completed because of the power limits imposed by existing laser equipment. The pulsed experiments show that the process should operate as a cw, gas entrained process with approximtely a 1.5 kw laser. These power levels are readily available with commerical equipment.

Both approaches for producing superior powders for Si_3N_4 ceramic bodies have been successfully demonstrated. The direct synthesis of uniform particle size powders appears more important than the comminution process. Also it can be explored with existing laser equipment, without imposing any serious limitations. Therefore, we will focus on direct synthesis of Si and Si_3N_4 powders during the second year of this program.

References

1. R. L. Coble, Proc. of the 4th Intl. Conf. on Reactivity of Solids, Amsterdam, 1960.

2. S. Prochazka and C. Greskovich, Bull. Amer. Ceram. Soci., 57, 579-81, 586 (1978).

3. A. Kato, Y. Ono, S. Kawazoc and I. Mochida, Yogyo Kyokai Shi, 80, 114-120 (1972).

4. J. Caneloup and A. Mocellin, in Special Ceramics, Vol. 6, Ed., P. Popper, pp. 209-222, 1975.

5. G. Heidemane, Tezisy Dokl-Konf., Molodykh Nauch. Rab. Inst. Neorg. Khim., Akad. Nauk Latv. SSSR, 4th Ed., Yu. N. Sokolov, Riga, USSR, pp. 38-39 (in Russian), 1975.

6. C. D. Greskovich, S. Prochazka and J. H. Rosolowski, Basic Research on Technology Development for Sintered Ceramics, G. E. Research and Development Laboratory under contract with the AF Materials Laboratory, Report AFML-TR-76-179, November, 1976.

7. P.E.D. Morgan, "Production and Formation of Si_3N_4 from Precursor Materials," Report # A-C3316, March 1973-December 1973.

8. C. H. Tindal, J. W. Straley, and H. H. Nielsen, Physical Review, 62, 151-159 (1942).

9. J. S. Garing, H. H. Nielsen and K. Narahorn, J. Molecular Spect., 3. 496-527 (1959).

10. R. R. Patty, G. M. Russwurm and D. R. Morgan, Applied Optics, 13, 2850-54 (1974).

11. C. Reiser, F. M. Lussier, C. C. Jensen and J. I. Steinfeld, J. Am. Chem. Soc. (in press).

12. B. D. Cullity, Elements of X-ray Diffraction, Addison-Wesley Publ. Co., Inc., Reading, Mass., p 261, 1956.

13. E.A. Taft, J. Electro. Chem. Soc.: Solid State Sc., 118, 1341 (1971).

14. H. C. Vande Hulst, Light Scattering by Small Particles, John Wiley and Sons, Inc., N. Y. (1957).

15. F. Reizman and W. Van Gelder, Solid State Electronics, 10 (7), 625-632, (1967).

16. F. A. Williams, Int. J. Heat Mass Transfer, 8, 575-587 (1965).

17. S. L. Glicker, Appl Oct., 10, 644-650 (1971).

18. B. Paul, ARS Journal, Sept. 1962, pp. 1321-1327.

19. L. D. Dickson, Appl. Optics, 9, 1954-61 (1970).

20. JANAF Thermochemical Tables, NSRDS-NBS37 (1971).